Charles University

Faculty of Science

Study programme: Analytical chemistry

Mgr. Barbora Štádlerová

Atomic fluorescence spectrometry with volatile species generation – a sensitive tool for ultra-trace elemental analysis

Atomová fluorescenční spektrometrie s generováním těkavých specií – citlivý nástroj pro ultrastopovou prvkovou analýzu

Doctoral thesis

Supervisor: RNDr. Stanislav Musil, Ph.D.

Supervisor-consultant: RNDr. Jakub Hraníček, Ph.D.

Supervisor-consultant: prof. RNDr. Jiří Dědina, CSc., DSc.

Prague 2024

Tato disertační práce byla vypracována na Ústavu analytické chemie AV ČR, v. v. i., Detašovaném pracovišti – Oddělení stopové prvkové analýzy v Praze.

Disertační práce byla finančně podporována Univerzitou Karlovou (projekt GA UK č. 1048120) a projektem SVV 260560, Grantovou agenturou České republiky (projekt č. 17-04329S, 19-17604Y a 23-06530S) a Ústavem analytické chemie AV ČR (výzkumný záměr RVO: 68081715).

Prohlášení

Prohlašuji, že jsem tuto závěrečnou práci zpracovala samostatně a že jsem uvedla všechny použité informační zdroje a literaturu. Tato práce ani její podstatná část nebyla předložena k získání jiného nebo stejného akademického titulu.

Jsem si vědoma toho, že případné využití výsledků, získaných v této práci, mimo Univerzitu Karlovu v Praze je možné pouze po písemném souhlasu této univerzity.

V Praze dne

. . . . . .

podpis

Poděkování

Ráda bych tímto poděkovala především svému školiteli RNDr. Stanislavu Musilovi, Ph.D. za vedení disertační práce, odborné rady, podporu a veškerý čas, který mi během mého doktorského studia věnoval. Dále bych ráda poděkovala svému konzultantovi prof. RNDr. Jiřímu Dědinovi, CSc., DSc. za cenné rady a pomoc v průběhu studia a všem zaměstnancům Oddělení stopové prvkové analýzy, Ústavu analytické chemie AV ČR, za spolupráci. V neposlední řadě patří dík za podporu během studia mé rodině a přátelům.

Prohlášení o autorství

Jako zástupce spoluautorů prohlašuji, že se Mgr. Barbora Štádlerová podílela na níže uvedených publikovaných pracích mírou uvedenou v závorkách:

B. ŠTÁDLEROVÁ, M. KOLROSOVÁ, J. DĚDINA, S. MUSIL: Atomic fluorescence spectrometry for ultrasensitive determination of bismuth based on hydride generation – the role of excitation source, interference filter and flame atomizers. Journal of Analytical Atomic Spectrometry, 35 (2020), 993–1002, DOI: 10.1039/d0ja00043d.

[60 %]

J. VYHNANOVSKÝ, D. YILDIZ, **B. ŠTÁDLEROVÁ**, S. MUSIL: Efficient photochemical vapor generation of bismuth using a coiled Teflon reactor: effect of metal sensitizers and analytical performance with flame-in-gas-shield atomizer and atomic fluorescence spectrometry. Microchemical Journal, 164 (2021), 105997, DOI: 10.1016/j.microc.2021.105997.

[35 %]

B. ŠTÁDLEROVÁ, J. DĚDINA, S. MUSIL: Comparison of bismuth atomic lamps for a non-dispersive atomic fluorescence spectrometry. Spectrochimica Acta Part B: Atomic Spectroscopy, 205 (2023), 106692, DOI: 10.1016/j.sab.2023.106692.

[80 %]

B. ŠTÁDLEROVÁ, L. SAGAPOVA, S. MUSIL: Chemical vapour generation assisted by Cr^{3+}/KCN coupled to atomic fluorescence spectrometry for ultrasensitive determination of cadmium in water and rice samples. Journal of Analytical Atomic Spectrometry, 38 (2023), 1213–1223, DOI: 10.1039/d3ja00083d.

[65 %]

. . . . . .

RNDr. Stanislav Musil, Ph.D.

Abstrakt

Tato disertační práce se zabývá vývojem nových analytických metodologií založených na atomové fluorescenční spektrometrii – detekční metodě, která nabízí precizní a citlivé stanovení ultrastopových prvků, mezi něž patří například bismut, kadmium a nikl. Společným jmenovatelem této práce je použití nekomerčního nedisperzního atomového fluorescenčního spektrometru (AFS) vyvinutého v laboratoři.

První část této práce se věnuje vývoji vysoce citlivé metody pro stanovení bismutu pomocí generování hydridů (HG) ve spojení s AFS. Bismutan byl generován reakcí s $NaBH_4$ v prostředí HCl v uspořádání průtokové injekční analýzy a pomocí proudu nosného plynu argonu a vodíku byl unášen do atomizátoru. Byla provedena detailní optimalizace optické cesty spektrometru (pozice bezelektrodové výbojky, čoček a interferenčního filtru) a atomizačních podmínek ve dvou plamenových atomizátorech – miniaturním difúzním plamenu (MDF) a tzv. flame-in-gas-shield atomizátoru (FIGS). Bylo dosaženo výborné opakovatelnosti a extrémně nízkých mezí detekce, jmenovitě 1,8 ng l^{-1} s využitím MDF a 0,9 ng l^{-1} s FIGS.

Následně byl AFS spojen s fotochemickým generátorem těkavých specií (PVG), opět v uspořádání injekční průtokové analýzy. Použitý fotoreaktor se skládal ze standardní rtuťové nízkotlaké UV výbojky ovinuté teflonovou trubičkou. Optimální podmínky pro PVG bismutu odpovídaly průtoku reakčního média 3 ml min^{-1} (doba ozařování 90 s) a reakčnímu médiu složeného ze směsi kyseliny octové a mravenčí s přídavkem Co^{2+} iontů jako modifikátoru. Atomizační podmínky ve FIGS atomizátoru byly zoptimalizovány a nijak významně se nelišily od optimálních podmínek pro HG-AFS, s výjimkou významně vyššího průtoku kyslíku. Mez detekce dosažená s PVG-AFS byla 12 ng l^{-1}.

Také byla vyvinuta metoda pro stanovení kadmia pomocí chemického generování těkavých specií (CVG) spojeného s AFS s využitím bezelektrodové výbojky jako excitačního zdroje. Těkavé specie kadmia byly generovány ve čtyřkanálovém průtokovém injekčním uspořádání generátoru reakcí s $NaBH_4$ v prostředí HCl za přítomnosti Cr^{3+}/KCN modifikátorů, jež zvyšují účinnost generování. Atomizační podmínky v obou plamenových atomizátorech byly zoptimalizovány a citlivost dosažená s FIGS atomizátorem byla přibližně dvakrát vyšší než s MDF, což vyústilo i v nižší mez detekce 0,42 ng l^{-1}.

Úpravou spektrometru a začleněním zdroje napájení pro výbojky s dutou katodou s vysokou září, tzv. Superlampy, byla rozšířena použitelnost AFS na větší počet analytů. Provozní parametry Superlampy byly optimalizovány s použitím bismutu jako modelového analytu se zřetelem na intenzitu emitovaného a výsledného fluorescenčního záření. Získané

analytické charakteristiky byly porovnány pro oba zdroje záření – bezelektrodovou výbojku a Superlampu.

Poslední část této práce je věnována vývoji metody pro stanovení niklu pomocí PVG-AFS s použitím Superlampy jako excitačního zdroje. Byl využit vysokoúčinný průtokový fotoreaktor s vnitřním reakčním kanálkem a těkavé specie niklu byly generovány z média obsahujícího kyselinu mravenčí při průtoku 1,5 ml min^{-1} odpovídající době ozařování 29 s. Atomizační podmínky byly zoptimalizovány pro MDF i FIGS atomizátory a s použitím FIGS atomizátoru bylo dosaženo meze detekce 5,3 ng l^{-1}.

Všechny vyvinuté metodologie byly ověřeny stanovením Bi, Cd a Ni v certifikovaných referenčních materiálech vody, vlasů a krve (Bi) a autentických vzorcích vody (Ni) a rýže (Cd).

Abstract

This thesis encompasses a development of innovative methodologies based on atomic fluorescence spectrometry, offering precise and sensitive determination of ultra-trace elements, such as bismuth, cadmium, and nickel. The common denominator of all parts of this work is the use of a research-grade non-dispersive atomic fluorescence spectrometer (AFS).

First part of this work is dedicated to the development of a highly sensitive methodology for bismuth determination based on hydride generation (HG) coupled with AFS. Bismuthane was generated by the reaction with $NaBH_4$ in HCl medium in a flow injection arrangement and directed by a stream of carrier argon and hydrogen to an atomizer. A detailed optimization of the optical path of the spectrometer (electrodeless discharge lamp, lenses and interference filter) and atomization parameters in two flame atomizers – miniature diffusion flame (MDF) and flame-in-gas-shield atomizer (FIGS) – was performed. An excellent repeatability and extremely low limits of detection were achieved, namely 1.8 ng L^{-1} with the MDF and 0.9 ng L^{-1} with the FIGS.

Subsequently, a photochemical vapour generation (PVG) of bismuth was coupled to AFS, employing a flow injection arrangement of the generator, a standard mercury low-pressure UV lamp and a coiled Teflon reactor. A flow rate of 3 mL min^{-1}, corresponding to an irradiation time of 90 s, and a combination of acetic acid and formic acid as the photochemical medium in the presence of Co^{2+} as a sensitizer were found optimal for PVG. The atomization conditions using FIGS atomizer were optimized and they did not differ significantly from HG-AFS, except for the significantly higher flow rate of oxygen. A limit of detection of 12 ng L^{-1} was achieved.

A methodology for cadmium determination based on chemical vapour generation (CVG) coupled with AFS using an electrodeless discharge lamp as the excitation source was also developed. Cd volatile species were generated in a four-channel flow injection CVG system by the reaction of the analyte with $NaBH_4$ in a HCl medium in the presence of Cr^{3+}/KCN as modifiers enhancing the CVG efficiency. The atomization conditions were optimized for both MDF and FIGS atomizers. The sensitivity obtained with the FIGS atomizer was approximately twofold higher compared to that with the MDF atomizer; therefore, the FIGS atomizer was selected for further analytical applications, providing an excellent limit of detection of 0.42 ng L^{-1}.

To expand the applicability in terms of number of analyte elements, the spectrometer was modified to be operated with boosted discharge hollow cathode lamps also called Superlamps. The operational parameters of the Superlamp were optimized using bismuth as the

model analyte with respect to the intensity of the emitted radiation and the resulting fluorescence radiation. The achieved analytical characteristics were compared for both excitation sources - electrodeless discharge lamp and Superlamp.

Last part of this thesis is dedicated to the development of a method for nickel determination based on PVG and AFS using the Superlamp as the excitation source. The PVG was conducted with a high-efficiency flow-through photoreactor from the photochemical medium containing formic acid at the flow rate of 1.5 mL min^{-1} through the photoreactor, which corresponds to an irradiation time of 29 s. The atomization conditions in both MDF and FIGS atomizers were optimized and a limit of detection of 5.3 ng L^{-1} was achieved with the FIGS atomizer.

Last but not least, all the developed methodologies were verified by the determination of Bi, Cd and Ni in certified reference materials of water, hair, and blood (Bi) and real samples of water (Ni) and rice samples (Cd).

Table of contents

List of abbreviations

AAS	atomic absorption spectrometer/spectrometry
ABC	analyte-borane complex
AF	atomic fluorescence
AFS	atomic fluorescence spectrometer/spectrometry
CD	capillary distance
CRM	certified reference material
CVG	chemical vapour generation
EDL	electrodeless discharge lamp
FA	formic acid
FI	flow injection
FIGS	flame-in-gas-shield
FWHM	full width at half maximum
HCL	hollow cathode lamp
HG	hydride generation
ICPAES	inductively coupled plasma atomic emission spectrometer/spectrometry
ICPMS	inductively coupled plasma mass spectrometer/spectrometry
LOD	limit of detection
LOQ	limit of quantification
MDF	miniature diffusion flame
MS	mass spectrometer/spectrometry
OH	observation height
PEEK	polyetheretherketone
PMT	photomultiplier tube
PP	peristaltic pump
PTFE	polytetrafluoroethylene
PVG	photochemical vapour generation
RC	reaction coil
RM	reference material
SD	standard deviation
SNR	signal-to-noise ratio
SRM	standard reference material
THB	tetrahydridoborate

UV	ultraviolet
vis	visible
VG	vapour generation

Aims of the thesis

The presented thesis summarizes the results from four research papers published in international impacted scientific journals with the addition of one yet unpublished study. The introduction briefly describes the theoretical aspects of this work and is focused mainly on various vapour generation techniques, flame atomizers used for the atomization of volatile species and atomic fluorescence spectrometry used for the detection. The experimental part lists the employed instrumentation including the measurement procedure and data treatment. The detailed description of the used reagents, instrumentation, sample preparation, etc., can be found in corresponding appendices. The individual sections in the results chapter are focused on the most important results that were especially related to the optimization of AFS and flame atomizers, the determination of analytical figures of merit and method validation, wherein some specific details can be found in the attached appendices.

The main aims of this thesis were to contribute to the development of the method of AFS coupled to chemical or photochemical vapour generation techniques and expand this methodology for the determination of transition metals. The individual sub-aims were:

a) to develop analytical methodologies for Bi determination using a research-grade atomic fluorescence spectrometer by the coupling with different vapour generation techniques and employing different excitation sources

- the determination of Bi by hydride generation (HG) coupled with AFS using an electrodeless discharge lamp (EDL) as the excitation source (Appendix I)
- the coupling of photochemical vapour generation (PVG) of Bi to AFS (Appendix II)
- the development and testing of a power source for high intensity hollow cathode lamps (Superlamps) in the research-grade AFS in order to expand the applicability of the spectrometer to other than only hydride forming elements (Appendix III)

b) to develop a sensitive methodology for Cd determination based on chemical vapour generation (CVG) coupled with AFS using EDL and the excitation source (Appendix IV)

c) to develop a sensitive methodology for Ni determination by coupling the PVG of Ni to AFS using the Superlamp as the excitation source (unpublished results).

1 Introduction

1.1 Trace element analysis

Many elements occur in various matrices at very low concentration levels, which, for a long period of time, made their determination virtually impossible. Their presence became known and the levels at which they can be found became detectable with the development of analytical instrumentation and hence the term "trace element" began to be used for their description. "Trace element", as defined by IUPAC [1], is any element having an average concentration of less than 100 mg kg^{-1}. Another term - "ultra-trace elements" - was established with further improvements of analytical techniques and the effort to lower their limit of detection (LOD) for elements occurring at lower levels than 1 ppm, even though it is not a rigid definition [1-3]. Such low concentrations of various elements might be either hazardous or essential to human health or the environment, depending on their character [4-6]. Regarding the analytes studied in this thesis, cadmium is a representative of thoroughly studied and monitored elements that are considered serious hazardous toxic pollutants [7, 8]. Cadmium is accumulated and therefore its concentrations in the environment are steadily increasing, mostly coming from battery production, alloys or fertilizers [9, 10]. Bismuth and nickel are less toxic than Cd, however, with an ongoing technological development and an increasing manufacturing capacities of various electronic devices, their level might be increasing in the future, potentially causing harm to the biosphere [11, 12]. Therefore, it is crucial to continue improving the performance of different analytical methodologies and especially try to stay ahead of the demand by predicting the global trends in element analysis.

Nowadays, methods of analytical atomic spectrometry are the methods of choice for trace or ultra-trace element analysis, which include atomic absorption spectrometry (AAS), AFS, inductively coupled plasma with atomic emission spectrometry (ICPAES) or inductively coupled plasma with mass spectrometry (ICPMS). Sample introduction has been always considered as the Achilles´ heel of all these methods [13], typically relying on nebulization of liquid samples with a limited introduction efficiency (<5%). It is possible to employ alternative sample introduction techniques, e.g., vapour generation (VG) [14] or laser ablation [15], to augment the analytical performance of the aforementioned methods. VG techniques can introduce the analyte into the detector with much higher efficiency than nebulization, in principle even up to 100%. They include chemical vapour generation (CVG), photochemical vapour generation (PVG), electrochemical hydride generation, plasma-assisted vapour

generation, sono- and thermochemical vapour generation. Hydride generation (HG) is technically a part of CVG when tetrahydroborate (THB) is used for the formation of volatile hydrides [14].

The VG techniques further discussed in this thesis include namely HG, CVG, and PVG. All of the VG techniques are based on the formation of volatile species of the analyte, which requires an appropriate atomizer to convert volatile species to free atoms prior to detection. The atomizers further discussed thus include two types of flame atomizers - the miniature diffusion flame (MDF) and the flame-in-gas-shield atomizer (FIGS), both designed specifically to be employed in AFS.

1.2 Vapour generation techniques

VG techniques coupled with various atomic spectrometric methods were introduced more than 50 years ago [16, 17]. The increase in their popularity over the years may be attributed to simple and affordable instrumentation and the corresponding analytical characteristics, especially very low LODs, going hand in hand with high analyte introduction efficiency to the atomizer/detection unit. Another advantage lies in the separation of the analyte from the sample matrix, which minimizes interferences during spectrometric detection.

Generally speaking, VG is a process during which analytes, originally bound in the form of non-volatile compounds, are converted to volatile species, by means of chemical or physical processes, then released from the liquid phase to the gas phase [18] and transported to the atomizer/detector. VG techniques can be virtually described by two stages: the formation of volatile species of the analyte in a reactor (generator) and the subsequent atomization/detection, accomplished by an atomizer integrated within an atomic spectrometer. The overall generation efficiency is influenced by three consecutive processes: the conversion to the volatile species, the liquid-gas phase transfer of the volatile species and the transport of the volatile species to the atomizer/detection unit. Various approaches can be used for the conversion of the analyte to its volatile form, such as chemically by suitable chemical reagents (CVG), electrochemical derivatization, or radical-mediated derivatization that is applied in PVG or plasma-assisted VG [14].

1.2.1 Chemical vapour generation

CVG by the reaction with aqueous boranes used as derivative reagents (tetrahydroborate - THB, usually $NaBH_4$ or KBH_4) is one of the most popular and mature VG techniques [14, 18, 19]. Volatile species formed during the derivatization can be either hydrides of the so-called hydride-forming elements (As, Bi, Ge, Pb, Sb, Se, Sn, Te) [19] and/or free atoms in the case of Hg and Cd [20, 21].

Robbins and Caruso [22] were the first authors who proposed a reaction mechanism for HG. They postulated a simple reaction scheme for the THB/acid system (equation 1 and 2):

$$BH_4^- + H^+ + 3\ H_2O \rightarrow H_3BO_3 + 8\ H^\bullet \qquad (1)$$

The resultant atomic hydrogen subsequently reacts with aqueous ions of the element (E^{m+}) and form the volatile hydride:

$$E^{m+} + (m + n)H^\bullet \rightarrow EH_n + mH^+ \qquad (2)$$

This theory has been generally adopted and it became known as the “nascent hydrogen” mechanism [19, 23]. This hypothesis has been discussed thoroughly within the analytical community and it was later concluded by Dědina [24] that, in fact, there was no definite evidence that would either support or refute the “nascent hydrogen” hypothesis. Since then, a thorough review of borane complex chemistry literature, along with focused experiments using deuterium-labelled reagents, has helped clarify some controversial aspects of CVG mechanisms [25-27]. This resulted in definitively rejecting the "nascent hydrogen" theory and adopting a model based on the direct transfer of hydrogen from boron to the element through formation of analyte-borane complex intermediates (ABCs) [25, 28-30].

Study of the processes and mechanisms governing CVG by aqueous boranes is a very complex task in a real reaction system with many influencing parameters to be considered [31, 32]. The mechanistic studies can be divided into several steps: (a) studies on the hydrolysis of aqueous boranes and (b) studies on the mechanism of hydrogen transfer from the reaction environment to the analyte. Further parameters to consider while studying the HG mechanism

include interferences from foreign elements and the action of possible additives. In the case of THB, the single step reaction of hydrolysis (equation 1) is stoichiometrically correct yet it does not accurately depict the complex mechanism and kinetics involved in the hydrolysis of THB through reaction intermediates (equation 3).

$$BH_4^- + 3\ H_2O + H^+ \rightarrow \text{intermediates} \rightarrow H_3BO_3 + 4\ H_2 \qquad (3)$$

The hydrolysis of THB in acidic reaction media is a stepwise reaction that can be more accurately represented by the equations 4-7:

$$BH_4^- + H_3O^+ \rightarrow BH_3(H_2O) + H_2 \qquad (4)$$

$$BH_3(H_2O) + H_2O \rightarrow (H_2O)BH_2OH + H_2 \qquad (5)$$

$$(H_2O)BH_2OH + H_2O \rightarrow (H_2O)BH(OH)_2 + H_2 \qquad (6)$$

$$(H_2O)BH(OH)_2 \rightarrow B(OH)_3 + H_2 \qquad (7)$$

The BH_4^- anion and all the hydridoboron species formed during hydrolysis containing at least one B–H bond can be potentially active in CVG. Volatile hydrides are formed by direct transfer of hydrogen from boron to analyte atoms. The hydrogen transfer and hydride formation are stepwise processes, wherein the hydrogen atoms come from different borane molecules. The formation of intermediate hydrido-metal complexes, in which the ligands are replaced stepwise by hydrogen atoms (equation 8), and the hydrogen transfer take place through ABCs.

$$EL_n \rightarrow EHL_{n-1} \rightarrow EH_2L_{n-2} \rightarrow \text{---} \rightarrow EH_m \qquad (8)$$

To summarize, the results from References [23, 29-32] refute definitively the “nascent hydrogen” theory and support the hypothesis based on the direct transfer of hydrogen from boron to the analyte following the formation of ABC, in which different hydrogen atoms come from different borane molecules [14, 23].

It is worth mentioning that the reaction with THB is also used for generation of volatile species of transition and noble metals, such as Au, Ag, Co, Cu, Ni, Pd, Zn and other. However, the yielded generation efficiency is usually much lower despite the use of various reaction modifiers and modified generator designs [33-36].

The types of reactors used for both CVG and HG include the batch system and the flow systems - the continuous flow and the flow injection (FI) setups [37-40]. They all consist of the chemical manifold and the gas-liquid separator (GLS) used for the separation of generated volatile species of the analyte from the liquid matrix. In the batch reactor, the reaction is carried out by mixing all the reagents in one vessel that also serves as the GLS (the chemical manifold is not necessarily required), from which the volatile species is then transported by a carrier gas to the atomizer. Continuous flow reactors work with a constant supply of all the reagents propelled by peristaltic pumps [14]. In FI reactors, the sample is injected into the flow of a carrier liquid and mixed with other reagents including THB, which results in a peak shaped signal [38].

1.2.1.1 Hydride generation of bismuth

Bismuth is one of the classical hydride-forming elements and inorganic Bi^{3+} reacts with aqueous THB forming BiH_3 – bismuthane [25, 38, 40-42]. The generation efficiency of BiH_3 using analytical conditions was estimated to be above 95% and it tends to decrease as the mass concentration approaches a few mg L^{-1} due to the formation of non-volatile solid species and nanoparticles, assumed to be elemental bismuth, which can lead to a curvature of the calibration function at higher concentrations [40]. BiH_3 can be generated over a very broad acidity range with dilute solutions being more convenient from the viewpoint of blank levels and sensitivity since there is no critical effect of the HCl concentration on analytical signals [19, 38]. Bi^{3+} is reactive towards all products of THB hydrolysis and the concentration of THB used for the reduction is usually quite low compared to the other hydride-forming elements, in the range 0.1–1% (depending on the generator system) [43, 44].

1.2.1.2 Chemical vapour generation of cadmium

Cadmium has not been commonly listed among the classical hydride-forming elements and Hg that are amenable to HG. Nevertheless, since the CVG of Cd has been a subject of an extensive research in recent years, utilizing various approaches [21, 45-51], it appears now that a combination of atomic (Cd^0) and molecular (presumably CdH_2) volatile species is generated

during the CVG process [21, 45, 46, 52]. The proportion of these species and also the overall CVG efficiency depend profoundly on the experimental conditions, particularly the ratio of BH_4^-/acid (pH), and also the presence of dissolved oxygen in the reagents. However, the use of modifiers has been identified as crucial to substantially improve the CVG efficiency. In a recent study, Sagapova et al. [53] compared the performance of CVG of Cd using different modifiers, including Co^{2+} ions/ascorbic acid/thiourea, Ti^{3+} or Ti^{4+}/KCN, and Cr^{3+}/KCN. The most favourable outcomes in terms of CVG efficiency (55–66%), inter-day repeatability, and robustness were achieved with a four-channel system employing Cr^{3+}/KCN as modifiers, achieving LOD of 60 ng L^{-1} when using AAS and a quartz tube atomizer [53].

The exact mechanism by which this combination of modifiers enhances the CVG of Cd has not been fully elucidated. However, Yilmaz et al. [47] proposed in their pioneering work that in a slightly acidic medium, a $[Cr(CN)_6]^{3-}$ complex is generated online from $Cr(OH)_3$ in an excess of KCN before mixing with BH_4^-. This complex subsequently interacts with BH_4^- to produce reactive borane complex intermediates that can efficiently react with Cd^{2+} and convert it into volatile species with high efficiency [47].

1.2.2 Photochemical vapour generation

In contrast to other VG techniques, PVG is based on the photolytic generation of free radicals and solvated electrons in sample solutions containing photochemical medium exposed to ultraviolet (UV) radiation [54]. Historically, PVG is a rather new technique. It was first introduced in 2000 by Kikuchi and Sakamoto [55], who reported efficient reduction of Se(VI) in formic acid based medium in the presence of TiO_2 photocatalyst to yield SeH_2. This was followed by a publication by Guo et al. [56] that described an analytical perspective. PVG has been rapidly evolving over the past two decades and it nowadays provides successful analytical applications for around 25 elements (As, Sb, Bi, Ge, Se, Sn, Tl, Te, Fe, Co, Ni, Hg, Pb, Cd, Cu, Mo, W, Os, I, Br, Cl, Rh, Re, Ru, and Ir) [14, 57-60]. A typical experimental setup is very similar to CVG or HG except the chemical manifold is here replaced by a photoreactor comprising a UV source. PVG can be conducted in a batch generator but the flow setups are more common. In addition to the photoreactor, essential components include a peristaltic pump for the supply of the liquid sample and a GLS. Simple photoreactors typically consist of a low-pressure Hg discharge lamp and a conduit of UV transmissible material placed in close proximity to the source to permit irradiation of sample solutions primarily by 254 nm radiation [58]. Advanced thin-film flow-through photoreactors employ a modified low-pressure Hg discharge lamp wherein the sample is irradiated

in a synthetic quartz channel directly immersed in the discharge [61]. Since UV photons have only to pass the thin synthetic quartz wall of the inner channel, this photoreactor permits ready access to intense 185 nm radiation in addition to 254 nm.

The PVG mechanism is based on the photochemical decomposition of low-molecular-weight organic acids (formic, acetic, or propionic) contained in the photochemical medium by UV radiation, leading to the formation of highly reducing $H^{\bullet}$, $R^{\bullet}$, and $COO^{\bullet-}$ radicals and solvated electrons [56, 59]. These radicals interact with the target elements to form volatile species, which can be free atoms, hydrides, carbonyls, or alkylated compounds depending on the reaction medium used [54]. The generated volatile species are subsequently separated from the liquid sample matrix and transported with high efficiency to a suitable detector.

1.2.2.1 Photochemical vapour generation of bismuth

The feasibility of PVG of Bi was firstly demonstrated by Guo et al. in 2004 [56] within a 20 element study using a batch style UV reactor, followed by a more in-depth study by Zheng et al. in 2010 [62] who employed a more conventional PVG reactor consisting of a quartz tube wrapped around a 125 W high-pressure Hg UV lamp. A significant step forward was made by Gao's group [63-65] who found Fe^{3+} ions to enhance the PVG efficiency substantially in a system based on a thin-film flow-through UV reactor. The authors also identified the dominant product of PVG as $Bi(CH_3)_3$ when acetic acid was used as the photochemical medium. A further enhancement of the PVG efficiency was demonstrated using Co^{2+} ions as the sensitizer [66].

1.2.2.2 Photochemical vapour generation of nickel

Nickel was the second analyte (after Se) to which PVG was successfully applied. Guo et al. [67] used a PTFE tube wrapped around a Hg germicidal lamp and low-molecular-weight organic acids to generate volatile $Ni(CO)_4$. Significant enhancement was reported when the pH of the photochemical medium containing formic acid was adjusted by an addition of hydroxides or sodium formate [67-69]. Employing a thin-film flow-through photoreactor, Šoukal and Musil [70] achieved the PVG efficiency of 42% when PVG was conducted from 30% (m/v) formic acid while the PVG efficiency of around 75% was reported when pH of this photochemical medium was adjusted by an addition of 1.5 mol L^{-1} ammonium formate (pH increased to the value 2.6). However, these conditions did not provide any significant benefit to

analytical performance, especially due to increased analyte contamination and dilution of samples inherent to preparation in the photochemical medium [70].

1.3 Atomization of volatile species

In principle, VG techniques can be easily coupled to all methods of analytical atomic spectrometry, including AAS, AFS, ICPAES, and ICPMS, and the resulting sensitivity (in terms of LODs) is strongly related to the employed detector. VG has always been closely linked to AAS and with the emergence of other analytical atomic spectroscopy methods, VG applications followed suit. VG coupled to AFS has demonstrated its advantages over AAS in terms of LOD and linear dynamic range and its potential can be especially exploited when using mild atomization conditions. Therefore, AFS is primarily associated with VG nowadays and it has become a well-established technique and a strong competitor to AAS [71-73].

An ideal atomizer should ensure complete conversion of analyte volatile species into free atoms without any side reactions. Simultaneously, it should allow for a long residence time of free atoms in the observation volume to enhance sensitivity and for minimum atomization interference. The ideal atomizer should also be robust, avoid significantly contributing to the measurement noise and be fairly affordable [74]. The complete conversion of hydrides to free atoms can be explained by the radical theory, which is based on formation of an excess of $H^{\bullet}$ (compared to the concentration of volatile species) [75-77]. The analyte, in its volatile form, is then atomized by interactions with H radicals formed by reactions between H_2 (in an excess) and O_2. Once the free atoms are transported beyond the cloud of H radicals, they begin to decay. The optimization process consists of establishing how the relevant operational parameters influence the H radical distribution. However, it cannot be easily determined and therefore the crucial parameter is the concentration of free atoms of the analyte. The atomizers most often used in AFS include various types of flame atomizers, such as the miniature diffusion flame (MDF) and the flame-in-gas-shield atomizer (FIGS) [19, 74].

1.3.1 Miniature diffusion flame

The MDF is a conventional hydride atomizer for AFS in both commercially available [78] and laboratory-made [71, 72, 79] spectrometers. Its construction is quite simple, comprising a vertical support tube through which a mixture of Ar and H_2, containing the analyte volatile species,

is introduced [79]. Hydrogen burns in the ambient atmosphere forming the diffusion flame at the top of this tube. Hydrogen radicals are formed in the outer zone of the flame by reactions between H_2 and ambient O_2 and diffuse into the inner volume of the flame where the analyte volatile species is fully atomized. The outer hot shell of the flame acts as an efficient shield preventing the decay of H radicals and free atoms of the analyte in the inner volume of the flame by reactions with components from the ambient atmosphere. The sensitivity of MDF is mainly controlled by the total flow rate of flame gases and the composition of the Ar/H_2 mixture [74]. It is worth noting that some MDF applications do not use cylinder-supplied H_2 but rely only on H_2 generated from the hydride generator [78]. The total gas flow rate has two contradictory effects: it enhances the shielding of free atoms from chemical reactions but also causes dilution of the free atoms in the observed volume, which reduces sensitivity. Thus, the optimum total gas flow rate is a compromise between the shielding and the dilution. Additionally, the observation height, defined as the distance of the radiation beam axis above the support tube top is an important experimental parameter that has to be optimized.

In summary, the MDF atomizer offers highly efficient atomization of analytes with minimal free atom reactions within the observation volume, resulting in very low atomization interferences. The MDF is exceptionally user-friendly, providing excellent long-term signal stability, and is cost-effective in terms of both investment and operational expenses [74].

1.3.2 Flame-in-gas-shield atomizer

An advanced flame atomizer developed to be applied in AFS is a flame-in-gas-shield atomizer (FIGS) [74, 80], which has so far been used only in research grade AFS instruments [71, 72, 80-84]. It involves the same vertical tube (with the inlet of Ar, H_2 and analyte hydride) but there is also a centred capillary for O_2 delivery. At the top of this capillary, oxygen burns in the presence of excess H_2, creating a highly fuel-rich O_2/H_2 microflame. Within and in the close vicinity of this microflame, an inhomogeneous cloud of H radicals is formed, effectively atomizing the analyte hydride. To protect the H radicals and free analyte atoms from reacting with atmospheric O_2 and to prevent the ignition of a diffusion flame at the top of the support tube, high flow rates of shielding Ar are employed [72, 74].

The fundamental processes, i.e., production of H radicals, protection of free atoms from the ambient atmosphere and dilution of analyte in the observation volume of the flame, are all controlled by the composition and the flow rate of the Ar/H_2 mixture when MDF is employed. In

the FIGS atomizer, each of these processes can be independently controlled, which is its most significant advantage. Because there is always an excess of H_2 over O_2, the production of H radicals and temperature are both controlled mainly by the O_2 flow rate, while the flow rate of shielding Ar controls the isolation of free atoms from molecular O_2 in the ambient atmosphere. The dilution of the analyte is then regulated by the total gas flow rate of the flame gases [74, 80].

1.4 Atomic fluorescence spectrometry

AFS coupled to a VG technique has a potential to reach extremely low LODs at very low purchase and operating cost and therefore provides an attractive alternative even to ICPMS detection. Its use dates back to 1964, when Winefordner and Vickers [85] introduced it as a new analytical method.

Atomic fluorescence (AF) is a radiational deactivation process which occurs after the excitation of free atoms by the absorption of radiation of characteristic wavelength from an appropriate excitation source. The emitted fluorescence radiation can be of the same, longer or (rarely) shorter wavelength. When the excited atoms absorb and re-emit the same wavelength radiation, it is a resonance fluorescence. Non-resonance fluorescence occurs when the exciting and the observed lines are of different wavelengths, and the main categories are direct-line fluorescence (a common upper level of the exciting and the fluorescence lines) and stepwise-line fluorescence (upper levels of the exciting and the fluorescence lines differ), both of which exhibit longer wavelength of the emitted radiation. Another type of non-resonance fluorescence, anti-Stokes fluorescence, occurs when the wavelength of the fluorescence line is shorter [86].

The measured signal is determined as the value of the observed fluorescence radiant flux. Free atoms in the gas phase get excited by absorbing a portion of the radiant flux from the excitation source. Subsequently, a fraction of the absorbed energy is lost by collisions with other particles (fluorescence quenching) and a fraction is emitted when the atoms return to their lower energy state by fluorescence. The fluorescence radiation is emitted in all directions at an angle 4π and the signal is measured in the employed angle Ω. The fraction of re-emitted photons from the total number of absorbed photons is called the fluorescence quantum yield and is expressed as the ratio of the fluorescence radiant flux to the absorbed radiant flux. A simplified equation (equation 9) for the measured fluorescence flux is:

$$\Phi_F \propto \frac{\Omega}{4\pi} \varphi_F \phi_0 \chi l N \qquad (9)$$

, where φ_F is the quantum fluorescent yield, χ is atomic absorption coefficient, l is the path length and N is proportional to the concentration of ground state atoms in the sample. It can be concluded that the measured fluorescence signal is linearly proportional to the radiant flux of the excitation source ϕ_0 and, at very low concentration levels, when the radiant flux is not significantly attenuated by absorption of free atoms, to the concentration of free atoms [86].

The experimental setup of an AFS is very simple, it always consists of three components: the excitation source, the atomizer, and the detector. The main atomizers employed in AFS were individually treated in subsections 1.3.1 and 1.3.2. A photomultiplier tube is most often used as the detector [86], wherein non-dispersive instruments may employ an interference filter for the selection of detected wavelength [71, 78, 87-89] while dispersive spectrometers typically employ a monochromator to select the appropriate detection wavelength. Since the transmission of the light through the filter is significantly higher (>10%) compared to a monochromator, non-dispersive instruments provide higher sensitivity.

Since the introduction of AFS as an analytical method, mainly two types of line excitation sources have been used - the hollow cathode lamp [90], as well as its high intensity version, i.e., boosted discharge hollow cathode lamp [91], and the electrodeless discharge lamps (EDL) [92, 93], both of which were already regularly used in AAS [91, 94-96]. Nowadays, the EDLs contain a small amount of the target element or its volatile salt sealed in a quartz bulb, which is filled with an inert gas and placed within a radiofrequency generator. The principle of the emission of a characteristic line spectrum from the lamp lies in the ionization of the inert gas by a radiofrequency field and subsequent vaporization, atomization, and excitation of the element [97]. The boosted discharge hollow cathode lamp (Superlamp, as called by the Photron manufacturer) consists of an anode, a cylindrical cathode made of the element of interest and a second “hot” cathode. The normal sputtering discharge operates between the anode and the cylindrical cathode. The secondary discharge, facilitated by the secondary cathode, significantly enhances the excitation efficiency of the sputtered atoms. Notably, one of the key advantages of the Superlamp is its broad availability for various analytes and relatively rapid stabilization of its radiation intensity [98]. Conversely, EDLs are known for potentially providing higher radiation intensities but necessitate considerably longer stabilization times. Moreover, their utility is now limited to elements that form volatile hydrides, Hg, Cd, Cs, Rb and P [97].

2 Experimental

All the details about used reagents, manufacturers of instrumentation, sample preparation, etc., are provided in corresponding papers – Appendices I–IV. Only the information necessary for the understanding of the achieved results is given in the following sections.

2.1 Instrumentation

2.1.1 Atomic fluorescence spectrometer

An in-house assembled non-dispersive AFS was used as a detector throughout this work [71]. This spectrometer consists of three main components - excitation source, atomizer, and photomultiplier tube (PMT), a schematic is depicted in Fig. 1.

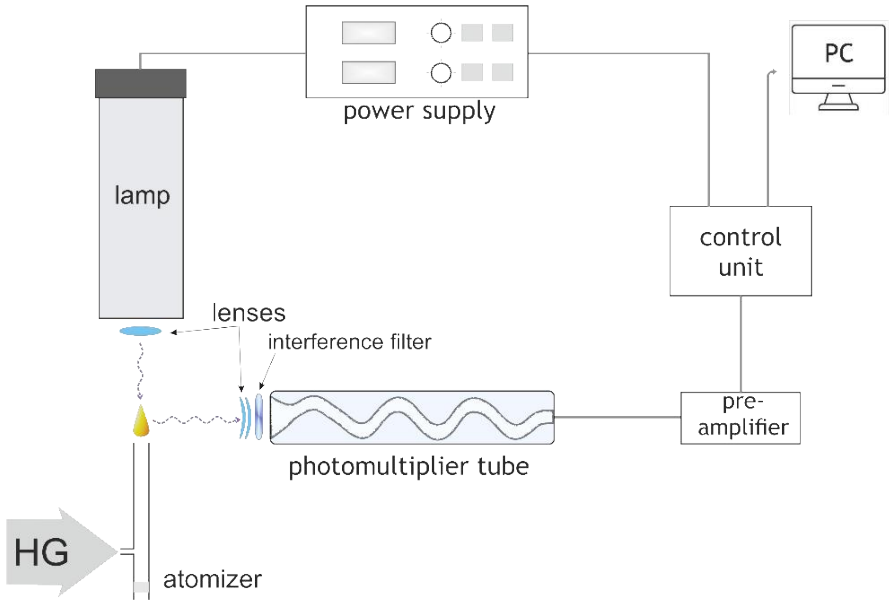

Fig. 1 Experimental setup of the research grade atomic fluorescence spectrometer.

An EDL of Bi and Cd (System 2, PerkinElmer, USA) and a Superlamp of Bi and Ni (Photron, Australia) were employed as the excitation sources. A commercial dual channel power supply source incorporating a radiofrequency lamp driver was used for operating the EDL. A power supply source for the operation and modulation of the primary current for the Superlamp was constructed by DIRAM company (Prague, Czech Republic). A commercial Superlamp power supply source (P200, 3 V, Photron, Australia) was used to add an arbitrary boost current on the Superlamp. This device allows only to transmit a boost current at the same modulation rate as used

for the primary current. The feeding current was square-wave modulated at frequency of 40 Hz for all the lamps and analytes. The duty cycle and the feeding current were the optimized parameters; the optimum settings are summarized in Tab. 1. Moreover, the optical path was optimized, separately for each element and lamp type. It included the choice of lenses to focus the radiation from the source and tuning mutual distances between the lamp and the atomizer and the atomizer and the PMT. The radiation from the EDLs was focused onto the volume of the flame using a combination of two UV fused silica lenses: a planoconvex lens (d = 25 mm, focal length 40 mm) and a biconvex lens (d = 22 mm, focal length 45 mm). The Superlamps were placed in a plastic tube of the same dimensions as the EDLs and a UV fused silica planoconvex lens (d = 25 mm, focal length 40 mm), in a circular holder, was attached to the rim of this tube. A solar blind PMT (165–320 nm, MH 1922, PerkinElmer, Germany) was placed perpendicularly to the excitation source and the produced fluorescence radiation was focused onto the interference filter using two positive meniscus lenses. The interference filters used for the selection of the desired wavelengths are given in Tab. 1. The full width at half maximum (FWHM) was 10 nm for all the filters.

Tab. 1 Optimal operational parameters of the excitation sources used in AFS and interference filters used

		Excitation source			**Interference filter**
	Lamp type	Feeding current (mA)	Boost current (mA)	Duty cycle (%)	Central wavelength (nm)
Bi	EDL	400	-	52	222.6; 307.1
	Superlamp	18	12	28	222.6; 307.1
Cd	EDL	240	-	52	228.0
Ni	Superlamp	19	26	52	232.0

2.1.2 Atomizers

Fig. 2a and 2b show the MDF and FIGS atomizers, respectively, used throughout this work. MDF consisted of a vertical quartz support tube (i.d. 6 mm) with a side inlet arm (2 mm i.d.) for the introduction of the volatile species of the analyte and the flame gases (Ar and H_2). The observation height (OH) was defined as the distance between the top of the support tube

and the centre of the radiation beam. FIGS consisted of the same support tube with a side inlet arm and, moreover, a quartz capillary (i.d. 0.53 mm) was added in the axis of the support tube for the introduction of O_2. The capillary distance, defined as the distance from the top of the capillary to the top of the support tube, was set as 3 mm, as depicted in Fig. 2b. A two-channel brass shielding unit [71] was fitted around the support tube and served to introduce the shielding (laminar) flows of Ar (inner $Ar_{shield\ I}$ and outer $Ar_{shield\ II}$). In this case, OH corresponded to the distance between the top of the capillary and the centre of the radiation beam.

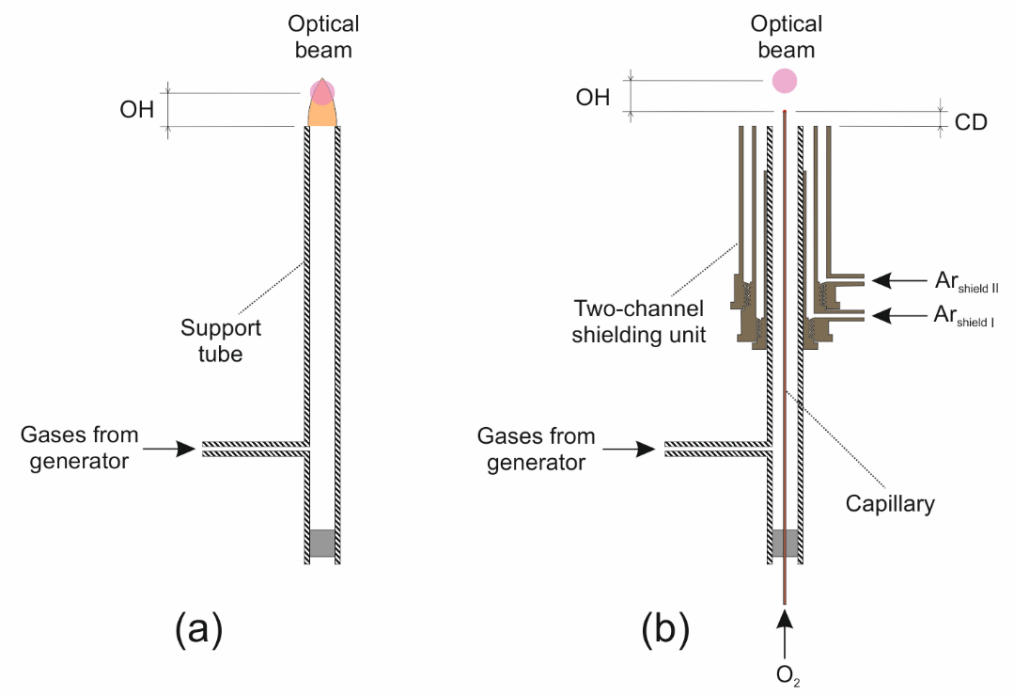

Fig. 2 MDF (a) and FIGS (b) atomizers; OH – observation height, CD – capillary distance.

2.1.3 Hydride generator for Bi

The same FI hydride generator as described previously [99], with only minor modifications, was employed for the generation of bismuthane (see Fig. 3). The chemifold was constructed using PTFE tubing (1 mm i.d.) with the exception of Tygon pump tubing. The continuous flows of the reductant (0.5% (m/v) $NaBH_4$ in 0.4% KOH, 1.2 mL min^{-1}) and the carrier (1 mol L^{-1} HCl, 4 mL min^{-1}) were maintained by a peristaltic pump (PP1). The sample (1 mL) was manually injected via an injection valve into the flow of the carrier and it was then mixed with the reductant. A glass GLS with forced outlet (5 mL volume) was used for separation of the gas phase containing the volatile species and the liquid phase, which was pumped by a peristaltic pump (PP2) to the waste. A 5 cm long PEEK capillary (0.25 mm i.d.)

was used for the introduction of the carrier gas - 80 mL min^{-1} of Ar ($Ar_{carrier}$) - in order to reduce the gas flow rate fluctuations caused by the formation of H_2 inside the reaction coil (11 cm). The flow rate of the H_2 evolving from the reaction inside the reaction coil corresponded to approximately 15 mL min^{-1} (measured under optimum HG conditions). The gas phase containing the analyte was supplied with an additional flow of Ar as well as H_2 in order to maintain a stable flame of the atomizer.

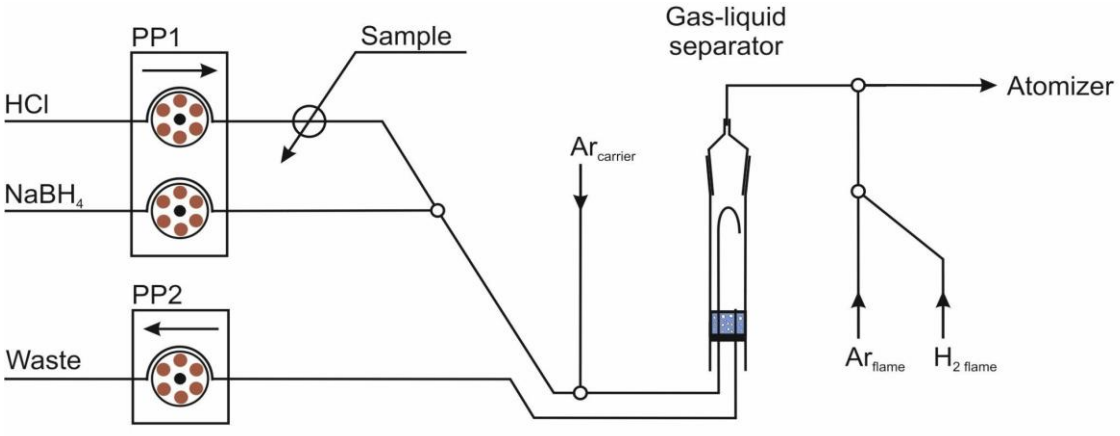

Fig. 3 Experimental setup of the hydride generator used for Bi; PP1,2 – peristaltic pumps.

2.1.4 Chemical vapour generator for Cd

A four-channel FI chemical vapour generator (Fig. 4) was used for the generation of Cd volatiles species, the design was taken over from the previous study by Sagapova et al. [53] and the conditions were slightly modified for the purpose of coupling this CVG to AFS. The carrier (0.2 mol L^{-1} HCl, 1 mL min^{-1}), the reductant (5% $NaBH_4$ in 0.4% KOH, 1 mL min^{-1}) and the solutions of modifier 1 and modifier 2 (0.6 mmol L^{-1} Cr^{3+} and 10 mmol L^{-1} KCN, both at 0.5 mL min^{-1}) were pumped using a peristaltic pump (PP1). The manifold was constructed from PTFE tubing and Tygon pump tubing. The standard/sample (prepared in 0.2 mol L^{-1} HCl) was injected through a 0.15 mL sample loop into the flow of the carrier and subsequently merged with the modifiers and the reductant in particular reaction coils (RC) as can be seen in Fig. 4. The volume of RC 1 and RC 2 (1 mm i.d.) corresponded to 63 µL. The volume of RC 3 was 932 µL (1.58 mm i.d.). A glass GLS (the same as described in subsection 2.1.3 for Bi) was employed for the separation of the Cd volatile species from the liquid waste. The flow rate of carrier Ar was 80 mL min^{-1} while the amount of H_2 evolving from the CVG reaction corresponded to ca. 20 mL min^{-1}. The gas phase leaving the GLS was supplied with an additional flow of Ar and H_2.

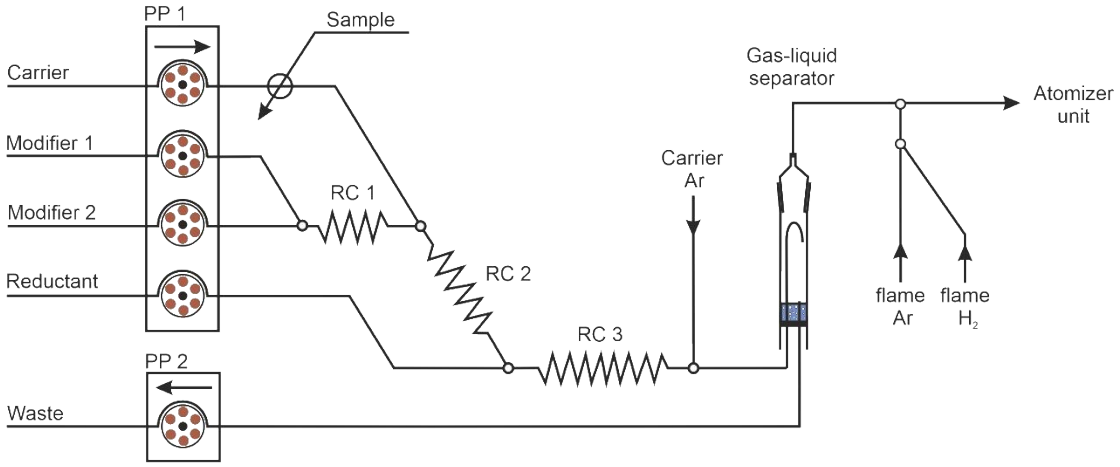

Fig. 4 Experimental setup of the four-channel chemical vapour generator used for Cd; PP1,2 – peristaltic pumps; RC 1, 2, and 3 – reaction coils.

2.1.5 Photochemical vapour generator for Bi

The FI photochemical vapour generator employed for Bi is shown in Fig. 5. The manifold was constructed using PTFE tubing (1 mm i.d.) and Tygon pump tubing. The photoreactor consisted of a 15W low-pressure Hg germicidal lamp whose circumference was wrapped around with 6 m length of PTFE tubing (irradiated volume 4.7 mL) through which the solution of the photochemical medium, a mixture of 40% (v/v) acetic acid and 1.25% (v/v) formic acid, was delivered by a peristaltic pump at the flow rate of 3 mL min^{-1}. The sample/standard (containing Co^{2+} as a sensitizer) was introduced into the stream of the carrier/medium through a 0.56 mL sample loop via an injection valve. The effluent from the photoreactor was carried by carrier Ar (100 mL min^{-1}) to a plastic GLS with forced outlet (15 mL volume), where the volatile species were separated from the liquid waste. The GLS was immersed in an ice bath in order to reduce the release of vapours from organic acids into the flame atomizer. For measurements with AFS, the gas phase leaving the GLS was supplied with an additional flow of Ar and H_2 in the same way as depicted in Fig. 3 and 4.

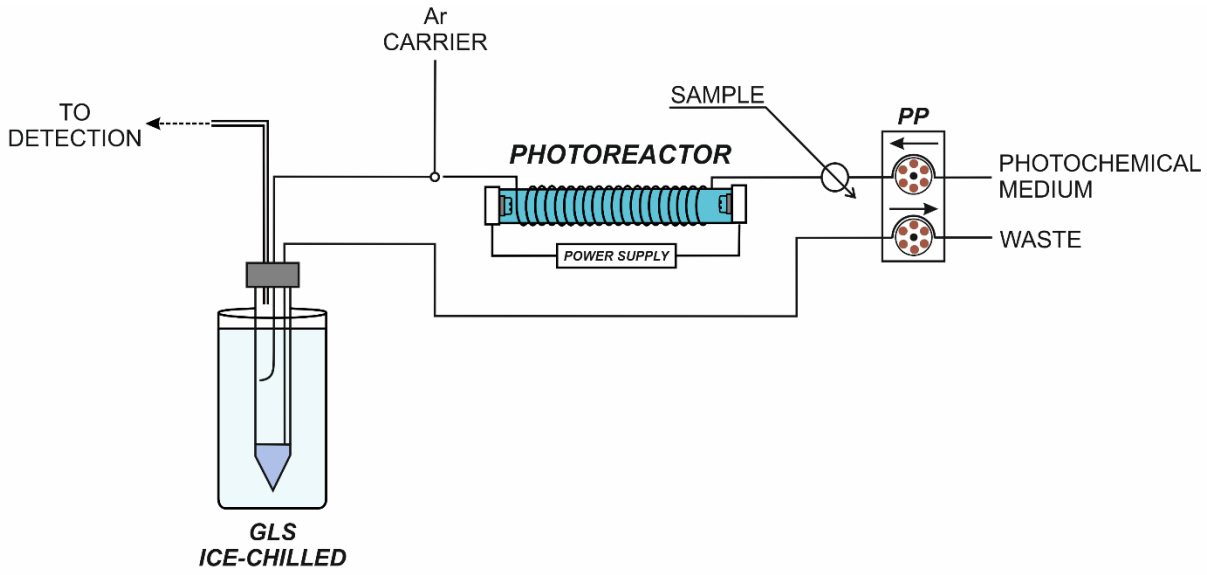

Fig. 5 Experimental setup of the photochemical vapour generator used for Bi; GLS – gas-liquid separator; PP – peristaltic pump.

2.1.6 Photochemical vapour generator for Ni

The FI photochemical vapour generator employed for Ni, taken over from Reference [70], is shown in Fig. 6. A thin-film flow-through photoreactor (Jitian Instruments Co., Beijing, China) was used. It comprises three lengths of synthetic quartz tubing (total volume 720 µL) inside the low-pressure Hg UV lamp (19 W) as well as two short quartz segments on either end of the photoreactor (250 µL) connecting the photoreactor to the chemifold. These quartz segments are not efficiently irradiated as the inner tubes immersed in the discharge. The photochemical medium, 30% (m/v) formic acid (purified by sub-boiling distillation), was being delivered by a peristaltic pump at the flow rate of 1.5 mL min^{-1}. The sample/standard solution (2 µg L^{-1} Ni; diluted from a 1000 mg L^{-1} stock solution, Analytika) was injected into the photochemical medium through a 0.51 mL sample loop via an injection valve. The effluent was mixed with a 200 mL min^{-1} flow rate of $Ar_{carrier}$ and carried to a plastic GLS with forced outlet (15 mL volume). The GLS was immersed in an ice bath in order to reduce the release of formic acid vapour into the flame atomizer. For measurements with AFS, the gas phase leaving the GLS was supplied with an additional flow of Ar and H_2 in the same way as depicted in Fig. 3 and 4.

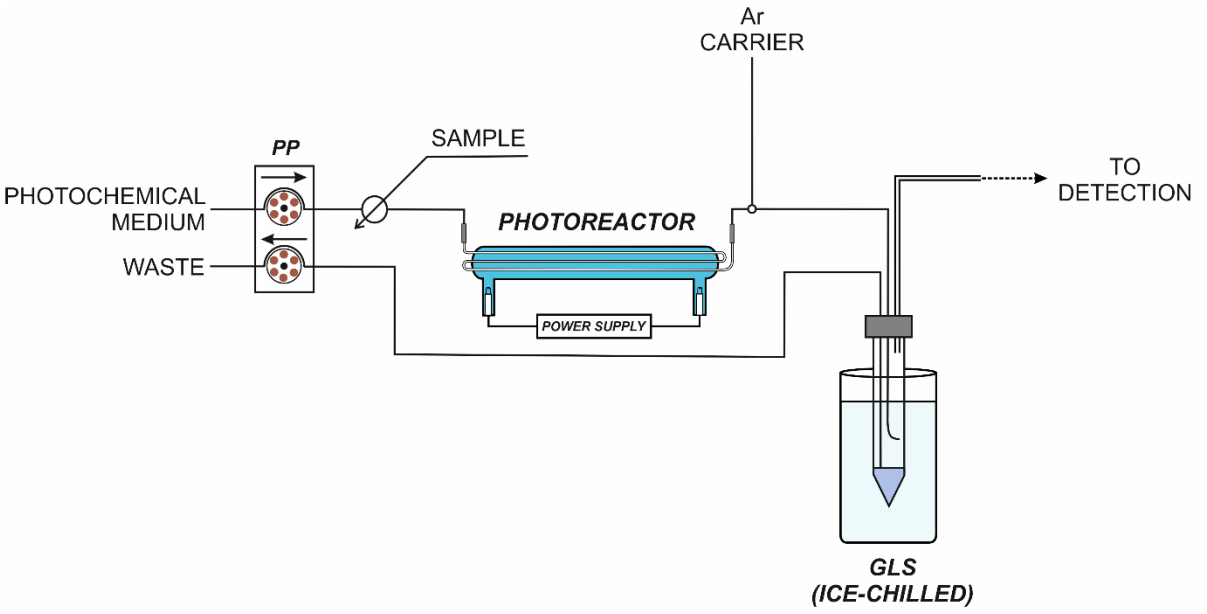

Fig. 6 Experimental setup of the photochemical vapour generator used for Ni; GLS – gas-liquid separator; PP – peristaltic pump.

2.1.7 Measurement procedure, data treatment and conventions

At the beginning of the measurement cycle, the recording of the signal from the PMT was initiated and followed by manual injection of the sample/standard into the flow of carrier. The recording of the signal time was stopped after the transient signal returned to the baseline. The recorded signals from the PMT were treated the same way as described previously [71, 72]. Basically, there are several factors contributing to the PMT response: the analyte fluorescence, the flame emission, the scattered radiation from the lamp, the parasitic radiation and the PMT dark current. The latter is so low for the particular PMT that it can be considered negligible especially when compared to the other factors mentioned. Furthermore, the spectrometer was placed inside a fume hood covered with a black curtain and thanks to that the contribution of the parasitic radiation was proven to be negligible. The feeding current of the excitation source was square-wave modulated at 40 Hz for all analytes, which allows for the detector to register the response in two channels - one registered when the lamp was on (channel 0; the analyte fluorescence, the flame emission, and the scattered radiation were detected) and the other when the lamp was off (channel 1; only the flame emission was detected). The resulting signal (in μV) reflects mainly the analyte fluorescence (and possibly the scattered radiation) and is obtained by subtracting the response from channel 1 from the

response from channel 0. Moreover, the influence of the scattered radiation is eliminated when peak area or peak height, both corrected to the baseline, are used for the evaluation.

The parameters used for data evaluation were the peak area (in μV s) or peak area sensitivity (in μV s L ng^{-1}) and specifically for HG of Bi also the peak height (in μV). Uncertainties are presented as ± standard deviation (SD) or combined SD where results are relative. Signal-to-noise ratio (SNR) was estimated by dividing the peak area, or peak height, by an uncertainty of the background level. The uncertainty of the background level was determined as an average of SDs of the background intensity (calculated from a certain number of values, details in the corresponding papers). LOD and LOQ was calculated as 3 × SD and 10 × SD, respectively, of peak area of blank ($n \geq 10$) divided by the slope of the calibration function.

In order to simplify the description of various gas supplies to the atomizer, the following conventions were established. The total flow rate of H_2 consists of the H_2 flow rate formed from the decomposition of $NaBH_4$ ($H_{2\ generator}$) and H_2 flow rate introduced downstream the GLS ($H_{2\ flame}$). The total flow rate of Ar consists of $Ar_{carrier}$, introduced upstream the GLS, and Ar_{flame}, introduced downstream the GLS. The total gas flow rate equals the sum of all of the above. The H_2 fraction is then the ratio of the total H_2 flow rate to the total gas flow rate.

3 Results

3.1 Atomic fluorescence spectrometry for ultra-sensitive determination of bismuth based on hydride and photochemical vapour generation (Appendices I–III)

The initial setup of a research-grade non-dispersive AFS was employed for As determination and its speciation analysis using HG as the sample introduction technique and the EDL as the excitation source [71, 72, 81-83]. The overall aim of this part of the thesis was to modify the arrangement and setting of this spectrometer and verify the feasibility of potential broadening of its applicability to a wider range of analytes.

Firstly, the spectrometer was configured for the determination of Bi employing HG and the EDL as the excitation source (Appendix I). Secondly, the AFS was coupled to alternative VG technique, i.e., PVG, that is capable of generating volatile species from a broader range of elements (Appendix II). Bi was employed as a model analyte again. In general, the paper

denoted as Appendix II deals with several couplings of PVG to sensitive analytical detectors (AAS, AFS, and ICPMS). The results dealing with optimization of PVG conditions for Bi using AAS and ICPMS as detectors are not discussed here because they were not the subject of the research in this thesis. Briefly, the optimum conditions for PVG of Bi were as follows: a mixture of 40% (v/v) acetic acid and 1.25% (v/v) formic acid and addition of 50 mg L^{-1} Co^{2+} as the sensitizer at a flow rate of 3 mL min^{-1} (irradiation time of 90 s) was found optimal, resulting in the overall PVG efficiency of 54 ± 2%. In both papers (Appendix I and II), the atomization conditions in two flame atomizers – MDF and FIGS were optimized, the analytical figures of merit were determined and the methodology was verified by the determination of Bi in several (certified) reference materials.

The spectrometer was further adjusted so that it could employ the Superlamp as the excitation source (Appendix III). This step was important as the market-availability of EDLs for various elements is limited and so by employing the Superlamp as the excitation source, the applicability of AFS may spread to, e.g., transition metals, when coupled with PVG.

3.1.1 AFS instrument

Commercially available AFS instruments usually employ the Superlamp as the excitation source. In contrast, the use of commercially available EDLs has appeared to be advantageous for laboratory-assembled instruments, thanks to their high radiation intensity, resulting in very low LODs as demonstrated in previous studies [71, 72]. The emission spectrum of the employed EDL obtained with a fibre optics UV-vis spectrometer revealed prominent bismuth emission lines (Fig. 7), specifically corresponding to the strong bismuth fluorescence lines that have been reported [86]. The corresponding emission lines were identified at 206.16, 222.82, 223.06, 302.46, and 306.77 nm.

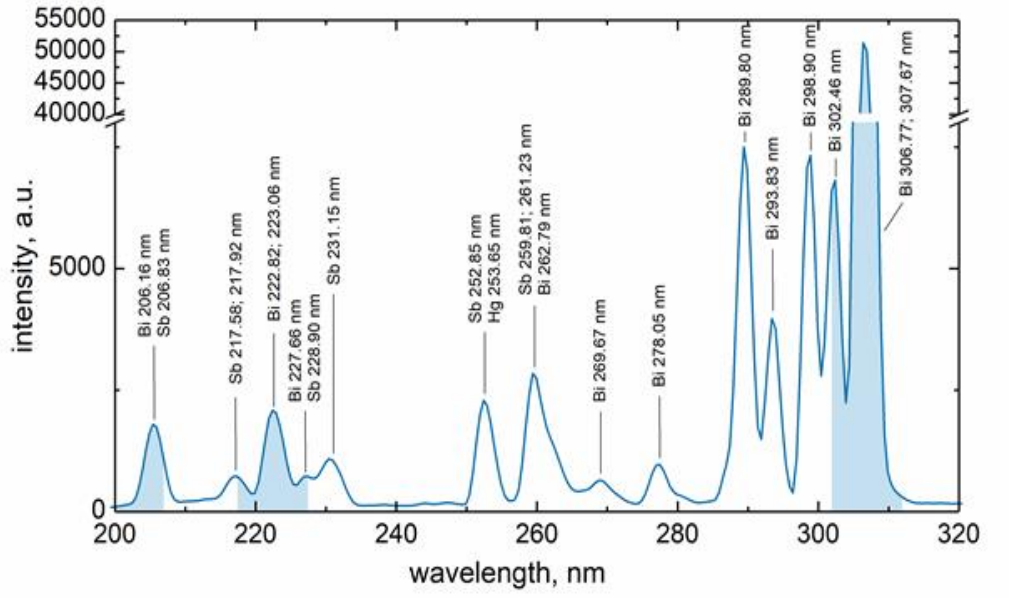

Fig. 7 Emission spectrum of Bi EDL (System 2; feeding current 400 mA) obtained with a fibre optics UV-vis spectrometer. Transmission bandwidth (FWHM 10 nm) of 202, 223 and 307 nm filters shown in colour for clarity.

Significant attention was directed towards the selection of an appropriate interference filter. Interference filters with central wavelengths at 193 (FWHM 20 nm), 202, 223, and 307 nm (FWHM 10 nm) were employed to cover the most intensive Bi fluorescence lines stated above, see Fig. 7 for a visual representation of transmission bandwidths of 202, 223, and 307 nm interference filters against the emission spectrum of the EDL. Generally, the transmittance profile of a filter influences both the sensitivity and the baseline noise. The sensitivity achieved when using a filter depends on the overlap of filter transmittance profile and the absorption profile of the electron transition associated with the excitation of a fluorescence line. It is important to note that the intensity of different Bi fluorescence lines varies and also the PMT response is not constant in its spectral interval of 165–320 nm. The maximum response is observed at ca. 200 nm and the response of the PMT then decreases at wavelengths both higher and lower than this point [100]. The sensitivities obtained with HG-AFS with various combinations of filter/atomizer are summarized in Tab. 2. The highest sensitivity was reached without the use of any filter (for both atomizers). However, this setup was not pursued any further since the determination would be then susceptible to interferences (no selection of detected wavelengths whatsoever). Another disadvantage of not using a filter is the need to perfectly isolate the spectrometer from the parasitic radiation from the laboratory environment. Naturally, the use of any filter reduced the achieved sensitivity. Filters 307 nm and 223 nm

provided sensitivity approximately one order of magnitude higher than 193 nm and 202 nm filters.

Tab. 2 Sensitivities (in mV s L μg^{-1}) for Bi determination obtained with HG-AFS with various interference filters and atomizers[a]

	193 nm filter	**202 nm filter**	**223 nm filter**	**307 nm filter**	**No filter**
MDF	0.014	0.011	0.13	0.17	2.3
FIGS	0.038	0.033	0.29	0.42	4.8

[a] experiment carried out under optimum conditions for both atomizers (Tab. 3)

While the sensitivity is certainly a relevant parameter, the SNR is the key factor for data evaluation in AFS. SNR is influenced by both sensitivity and baseline noise. The baseline noise depends on the overlap of the filter transmittance profile with the emission spectrum of the atomizer flame. Even though the flame emission is compensated for in the resulting signal (see subsection 2.1.7), its noise still contributes to the noise of the baseline. The OH radicals are responsible for the flame emission that is the most prominent in the wavelength range between 305 and 320 nm [84, 88]. When the two flame atomizers are compared, MDF produces significantly more OH radicals than FIGS, which results in approximately 1.9 times higher SNR achieved with the 223 nm filter compared to the 307 nm filter. On the other hand, SNRs of the two filters do not differ significantly using either the 223 or the 307 nm filter when FIGS is used due to lower amount of the OH radicals formed in the microflame. The other two filters (193 nm and 202 nm) provide approximately 6 times lower SNR than the two filters mentioned above. It is worth mentioning that Sb and Hg impurities were identified inside the EDL (see Fig. 7). These impurities result in serious positive interference from Sb on Bi determination with 202 nm and 223 nm filters, all details provided in Appendix I. However, this can be overcome by using the 307 nm filter as no Sb line is present in this region. In the end, FIGS as the atomizer and the 307 nm filter were finally chosen to be suitable for Bi determination in real samples.

It was important to optimize the optical path in order to gain the highest sensitivity and/or SNR by adjusting the mutual distances among the main components - the excitation

source, the atomizer and the PMT. The distance from the lens mounted on the rim of the EDL and of the PMT entrance lens to the centre of the support tube of the atomizer was set to 13 and 12 mm, respectively, which resulted in the radius of the radiation beam vertical cross-section above the vertical axis of the atomizer of approximately 5 mm. The lamp was operated at frequency of 40 Hz and 52% duty cycle [71, 72]. The feeding current of the EDL was optimized, the sensitivity increased with higher feeding current up to 425 mA, which was also the maximum value tested. However, the highest SNR was reached at 400 mA, which is also the recommended value of the manufacturer for this EDL for the modulated mode of operation.

3.1.2 Optimization of atomization conditions

3.1.2.1 Hydride generation of Bi

For the coupling of HG of Bi to AFS, the optimized atomization conditions included the H_2 fraction, the total gas flow rate, and the observation height for both atomizers. Another two parameters, the O_2 flow rate and the shielding Ar flow rate, were also optimized for FIGS. The 223 nm interference filter was used in all the optimizations, if not stated otherwise, in order to facilitate the experiments as it delivered sufficiently high SNR and sensitivity for both flame atomizers.

Generally speaking, decreasing the H_2 fraction in both atomizers positively influenced both the sensitivity and SNR (Fig. 8). This experiment was carried out at a constant flow rate of 600 mL min^{-1}, thus the change of sensitivity was driven solely by H_2 fraction. The sensitivity decrease at higher H_2 fraction may be explained by the Lorentz broadening of the absorption line as described for Se [101]. A broader absorption line results in a less effective excitation of free analyte atoms, leading to a reduced fluorescence signal. Furthermore, elevated temperatures associated with higher H_2 fractions inevitably decrease the fluorescence signal due to thermal expansion, although this effect can be partially counteracted by the Lorentz broadening decreasing at higher temperatures. Another mechanism possibly responsible for the decline in sensitivity with increasing H_2 fraction could be the quenching of the excited state of free bismuth atoms, either by H_2 or by produced water molecules in the flame. At a total gas

flow rate of 600 mL min^{-1}, the lowest feasible H_2 fraction in the MDF and FIGS setups corresponded to 14% and 9%, respectively, as flames exhibited instability at lower H_2 fractions.

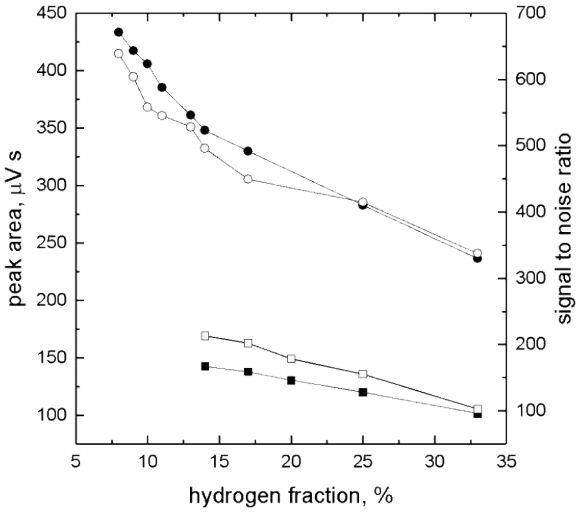

Fig. 8 Dependence of peak area (full circle) and SNR (empty circle) on H_2 fraction in MDF (square) and FIGS (circle); conditions for both MDF and FIGS: 1 μg L^{-1} Bi taken for HG, 600 mL min^{-1} total gas flow rate; for MDF: observation height of 7 mm; for FIGS: observation height of 6 mm, 7 mL min^{-1} oxygen flow rate, 1.5 ($Ar_{shield\ I}$) and 2 L min^{-1} ($Ar_{shield\ II}$) of shielding Ar.

The influence of the total gas flow rate and the observation height in MDF and FIGS at selected constant optimum hydrogen fractions of 17% and 13%, respectively, was investigated and is presented in Fig. 9 and Fig 10.

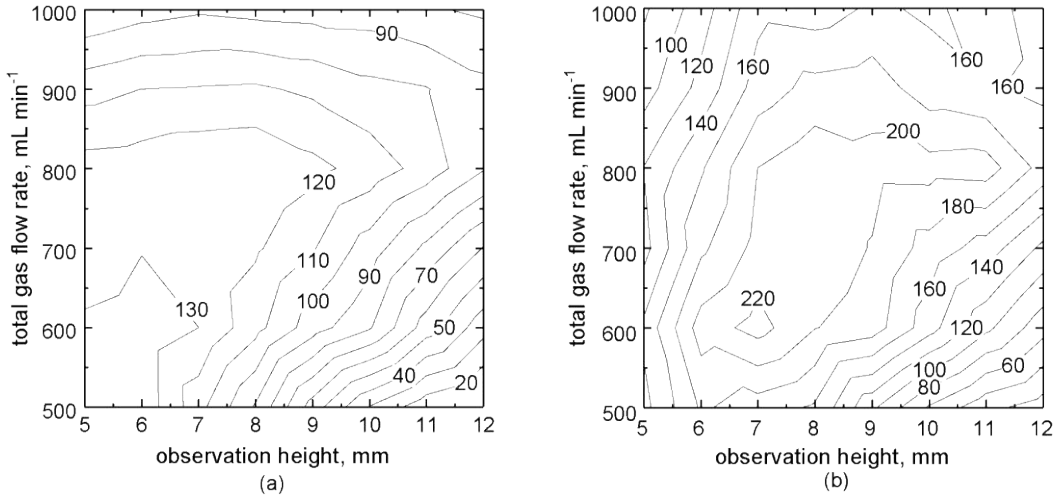

Fig. 9 Dependence of (a) peak area (in μV s) and (b) SNR on total gas flow rate and observation height in MDF; conditions: 1 μg L^{-1} Bi taken for HG, H_2 fraction 17%. The observation height points measured were in the range of 5–12 mm, by 1 mm. The total flow rate points measured were in the range of 500–1000 mL min^{-1}, by 100 mL min^{-1}.

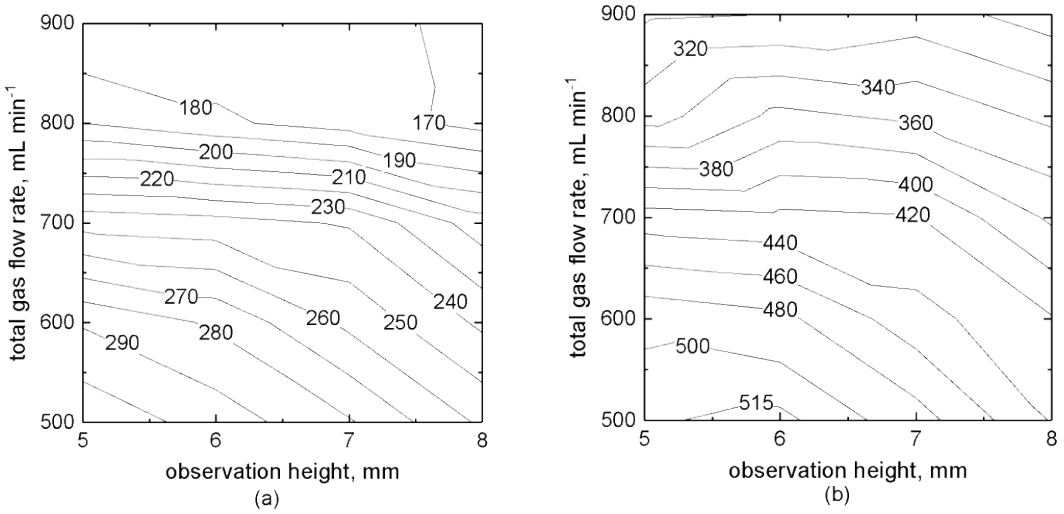

Fig. 10 Dependence of (a) peak area (in μV s) and (b) SNR on total gas flow rate and observation height in FIGS; conditions: 1 μg L^{-1} Bi taken for HG, H_2 fraction 13%, 7 mL min^{-1} oxygen flow rate, 1.5 ($Ar_{shield\ I}$) and 2 L min^{-1} ($Ar_{shield\ II}$) of shielding Ar. The observation height points measured were in the range of 5–8 mm, by 1 mm. The total flow rate points measured were in the range of 500–900 mL min^{-1}, by 100 mL min^{-1}.

It was not possible to use flow rates lower than 500 mL min^{-1} due to flame instability under the specified conditions. The minimum feasible observation height corresponded to 5 mm since at lower observation height values, the radiation from the EDL was considerably scattered on the top of the atomizer causing an undesirable increase of the background level. In both MDF and FIGS, the sensitivity decreases with an increase of the total gas flow rate and the observation height from the feasible minimums (Fig. 9 and 10). This trend can be explained by the dilution of free Bi atoms within the observation volume of the flame. The SNR in both atomizers is similar and it is negatively influenced by the background level increase, as well as baseline uncertainty increase, at observation heights below 7 mm for MDF and below 6 mm for FIGS. The optimized values for the total gas flow rate and the observation height are 600 mL min^{-1} and 7 mm for MDF, and 500 mL min^{-1} and 6 mm for FIGS (Tab. 3). Other parameters needed to be optimized for FIGS because of its more complex arrangement: O_2 flow rate and two shielding flows of Ar. The maximum sensitivity and SNR are achieved for 5–7 mL min^{-1} of O_2 being introduced through the capillary, as evident in Fig. 11. Lower flow rates are probably insufficient for an efficient atomization and higher flow rates cause greater water vapour formation, which can lead to fluorescence quenching and lower signal. Similar influence of O_2 flow rate was also observed when the 307 nm interference filter was used, the

highest sensitivity and SNR were reached at 7 mL min^{-1}, which was selected as optimum for further experiments. This finding confirms that the emission of OH bands in FIGS in the employed range of O_2 flow rate of 4–10 mL min^{-1} does not pose any problems.

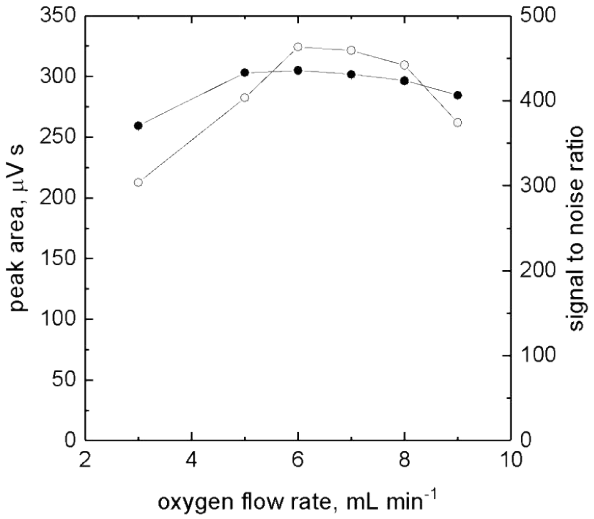

Fig. 11 Dependence of peak area (full circle) and SNR (empty circle) on O_2 flow rate in FIGS; conditions: 1 μg L^{-1} Bi taken for HG, 500 mL min^{-1} total gas flow rate, H_2 fraction 13%, 1.5 ($Ar_{shield\ I}$) and 2 L min^{-1} ($Ar_{shield\ II}$) of shielding Ar, observation height of 6 mm.

Last but not least, the two shielding Ar flow rates were optimized. The sensitivity and the highest SNR were achieved with 1.5 L min^{-1} in both inner and outer channels, and therefore, they were selected as optimal. The flow rate in the inner channel had a significantly greater impact on the resulting sensitivity than the flow rate in the outer channel, which can be documented by high relative sensitivities of 76%, 93%, and 96% reached using only the inner channel supplied with flow rates of 1, 1.5, and 2 L min^{-1}, respectively, compared to employing 1.5 L min^{-1} in both channels. The relative sensitivities achieved with only the outer channel were significantly lower, ranging 14–17%. The overall optimum conditions of atomization for both atomizers are summarized in Tab. 3.

Tab. 3 Optimum conditions of atomization of Bi in MDF and FIGS for HG-AFS

	Ar (mL min^{-1})	**H_2 (mL min^{-1})**	**O_2 (mL min^{-1})**	**$Ar_{shield\ I}$; $Ar_{shield\ II}$ (L min^{-1})**	**Observation height (mm)**
MDF	500	100	-	-	7
FIGS	440	60	7	1.5; 1.5	6

3.1.2.2 Photochemical vapour generation of Bi

PVG of Bi was coupled to AFS and both MDF and FIGS atomizers were tested for atomization of generated volatile species. The same parameters (SNR and sensitivity) were used for the data evaluation. The previous experiments with HG-AFS of Bi described in the subsubsection 3.1.2.1 demonstrated that overall better analytical characteristics were achieved with FIGS, however, MDF is generally considered to be more robust towards various interferences. This might be advantageous when, e.g., an organic acid based medium is used for PVG. The optimal conditions summarized in Tab. 3 were used as the default atomization conditions. Nevertheless, it was assumed that optimal atomization conditions might differ for HG and PVG approach, especially because of the different volatile species generated (BiH_3 for HG vs. $(CH_3)_3Bi$ for PVG [63, 64, 66]) and high concentration of organic acids (40% (v/v) acetic acid and 1.25% (v/v) formic acid) necessary for an efficient PVG of Bi. Despite only a little warming up of the medium occurring inside the coiled reactor (temperature rose up to 28 °C), vapours of the acids are continuously purged from the GLS by a stream of $Ar_{carrier}$. Karadjova et al. [102] proved a serious interference from organic solvents during atomization of AsH_3 in the MDF. Even the presence of low concentration of methanol, ethanol, or propanol in the HCl solution used for HG exhibited a serious suppression of sensitivity caused by the decrease of the atomization efficiency. This effect was attributed to the formation of carbon radicals and carbon particles causing a decay of the analyte free atoms and/or a reduction in the population of H radicals responsible for the atomization [102].

It was found out that the optimum atomization conditions using PVG with the MDF and 223 nm interference filter do not differ significantly from the optimum conditions using HG. Optimum total gas flow rate was 600 mL min^{-1} with H_2 fraction of 17% and observation height

of 6 mm. If the sensitivities (in μV s ng^{-1}) obtained with HG and PVG are to be compared for the evaluation of atomization efficiency, it is important to take into account different generation efficiencies of HG (above 90% expected) and PVG (=54%). The presence of organic acids vapours from the PVG showed relatively low suppression of the atomization efficiency in the MDF, ca. by 15%. On the other hand, the same comparison drawn for FIGS and the two generation techniques revealed decrease in atomization efficiency by 25% for PVG compared to HG. Karadjova et al. [102] used a similar type of atomizer as the FIGS atomizer and they reported that higher flow rate of added O_2 suppressed the extent of "carbon" interference. Subsequently, the effect of the H_2 fraction (Fig. 12a) and the O_2 flow rate through the capillary (Fig. 12b) were investigated in addition to the total gas flow rate and the observation height (Fig. 13). It was evident that the optimum conditions employing FIGS for PVG-AFS were different from HG-AFS. The most noticeable difference was that the optimum O_2 flow rate (see Fig. 12b) corresponded to 20 mL min^{-1} as opposed to 7 mL min^{-1} in the case of HG. Furthermore, the observation height then had to be elevated from 6 to 9 mm. Higher optimum O_2 flow rate corresponds to the findings of Karadjova et al. [102] and it provides better resistance towards the "carbon" interference. Lastly, the total gas flow rate had to be slightly adjusted - from 500 to 600 mL min^{-1} (Fig. 13) but the H_2 fraction remained the same (12%).

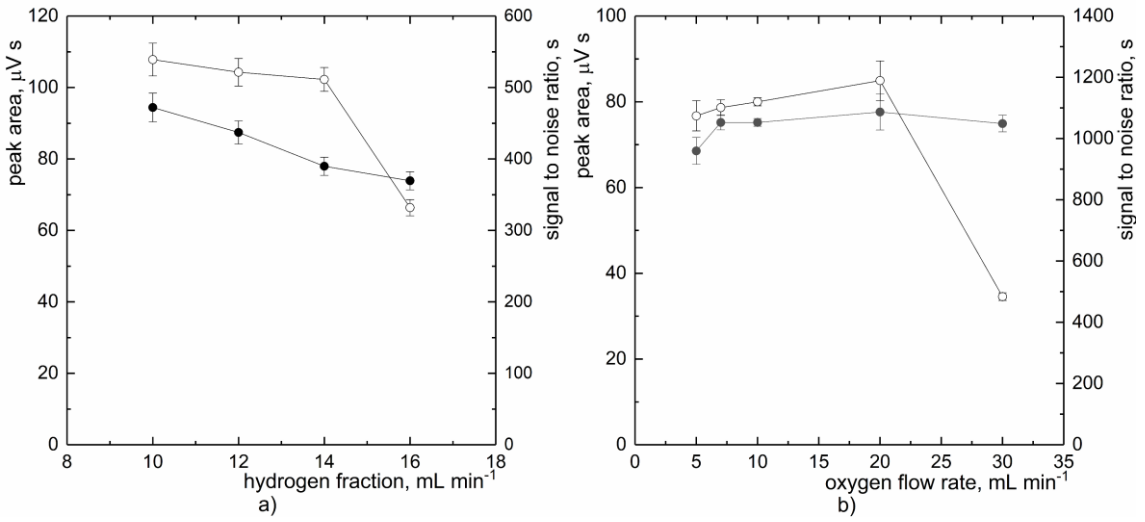

Fig. 12 Dependence of peak area (full circle) and SNR (empty circle) on H_2 fraction (a) and O_2 flow rate (b) in FIGS; conditions: 1 μg L^{-1} Bi taken for PVG, 500 mL min^{-1} total gas flow rate, H_2 fraction 12% (if not optimized), O_2 flow rate 20 mL min^{-1} (if not optimized), 1.5 ($Ar_{shield\ I}$) and 1.5 L min^{-1} ($Ar_{shield\ II}$) of shielding Ar, observation height of 6 mm.

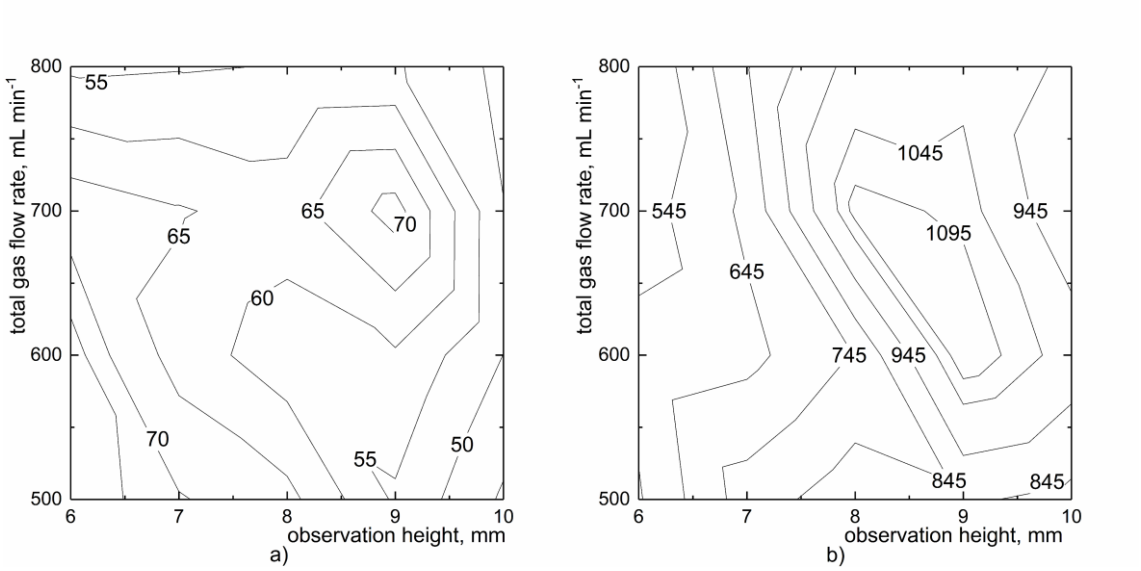

Fig. 13 Dependence of (a) peak area (in µV s) and (b) SNR (in s) on total gas flow rate and observation height in FIGS; conditions: 1 µg L^{-1} Bi taken for PVG, H_2 fraction 12%, 20 mL min^{-1} oxygen flow rate, 1.5 ($Ar_{shield\ I}$) and 2 L min^{-1} ($Ar_{shield\ II}$) of shielding Ar. The observation height points measured were in the range of 6–10 mm, by 1 mm. The total flow rate points measured were in the range of 500–800 mL min^{-1}, by 100 mL min^{-1}.

It seems that both MDF and FIGS are negligibly or just partly impaired by the presence of organic acid vapour released from the generator and the atomization efficiency still remains sufficiently high. Furthermore, it appears that it is not important which volatile species is introduced into the atomizer, whether BiH_3 in the case of HG or $(CH_3)_3Bi$ in the case of PVG [63, 64, 66]. The SNR achieved with FIGS was approximately 1.8 times higher than with MDF and therefore, FIGS was further used for the evaluation of the developed methodology using PVG-AFS and its application to the real samples. All the optimum atomization conditions are summarized in Tab. 4.

Tab. 4 Optimum conditions of atomization of Bi in MDF and FIGS for PVG-AFS

	Ar (mL min^{-1})	H_2 (mL min^{-1})	O_2 (mL min^{-1})	$Ar_{shield\ I}$; $Ar_{shield\ II}$ (L min^{-1})	Observation height (mm)
MDF	500	100	-	-	6
FIGS	528	72	20	1.5; 1.5	9

3.1.3 Optimization of the excitation sources - introducing the Superlamp

The general aim of this part was to adjust the laboratory-made AFS instrument so that it could employ the Superlamp as the excitation source, thus it could be employed for determination of other than only hydride forming elements, such as transition metals.

A significant part of this study was devoted to an examination and optimization of the operation of the Superlamp and its use for Bi determination by HG-AFS. The optimum atomization conditions from Tab. 3 were adopted, the Superlamp operation parameters were optimized and the resulting analytical performance was compared to that achieved with the EDL. It should be noted that the MDF atomizer was used throughout all the experiments with the Superlamp. As evident in Fig. 14, Bi Superlamp provides different emission spectra than Bi EDL (the green dashed line in Fig. 14). There are more emission lines present in the EDL spectrum and it has been proven that the Bi EDL contains especially Sb impurities responsible for emission lines at 206.8, 217.6, 217.9, 228.9, 231.2, 252.9, 259.8 and 261.2 nm and also Hg impurities responsible for the emission line at 253.7 nm. Firstly, the optical path was optimized in the same way as in subsection 3.1.1. Because of the different geometry of the Superlamp and the EDL, only one lens is needed for the focusing of the emitted radiation from the Superlamp, whereas a combination of two lenses (one inserted inside and one mounted on the rim of the exit orifice) are used for the EDL. The mutual distances among the Superlamp, the atomizer, and the PMT were set as follows: 20 mm distance between the lens mounted on the rim of the Superlamp and the axis of the vertical support tube of the atomizer and from there 12 mm distance to the lens of the PMT. This setup resulted in a circular vertical cross-section of the radiation beam above the atomizer of approximately 2 mm (as opposed to 5 mm in the case of EDL).

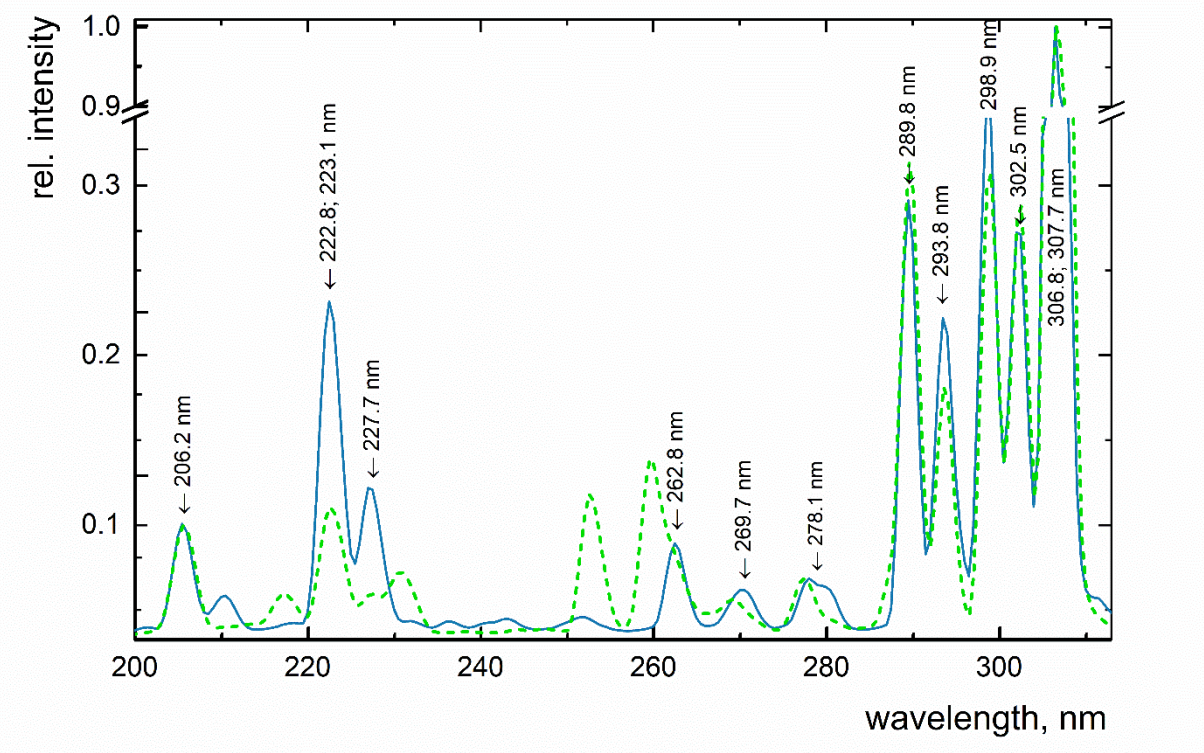

Fig. 14 Emission spectra of Bi Superlamp (blue line). Intensities shown are related to that of the most intensive line at 307 nm, the arrows indicate the most intense Bi lines of the Superlamp (here operated as HCL - primary current 12 mA). Emission spectrum of Bi EDL (green dashed line; 400 mA) is added for comparison (displayed also in Fig. 7). Note: the intensities of emitted radiation of both lamps were not recorded with the same geometry.

As mentioned in subsection 3.1.1, the optimal parameters for the EDL were as follows: the feeding current of 400 mA and 52% duty cycle (13 ms lamp on, 12 ms lamp off) at the frequency of 40 Hz. The parameters optimized for the Superlamp included the duty cycle, the primary current and the boost current. Firstly, it was found that for zero boost current, which means the Superlamp being operated as a standard HCL, the optimum primary current was 18 mA and the duty cycle was 28% (the lamp is on for 7 ms in a period of 25 ms). Primary current of 18 mA and boost current of 12 mA were selected as optimum resulting in a 4 times greater SNR than when zero boost current was employed. It was observed that the optimum boost current was higher at lower primary current values used. For example, when a primary current of 10 mA was used, the highest sensitivity and SNR were achieved with a boost current of 18 mA. Nevertheless, such parameters did not lead to any improvement. In subsection 3.1.1, the operating parameters of the EDL were optimized, which led to optimal performance being achieved with a 52% duty cycle along with a 400 mA power supply. Unlike the Superlamp,

a 28% duty cycle was not beneficial in any way for the EDL. The 52% duty cycle consistently provided higher sensitivity and more stable intensity of the emitted radiation. At 28% duty cycle, the baseline that represents the intensity of the emitted radiation (due to light scattering) kept drifting, requiring longer time to stabilize. The optimum conditions of operation the Superlamp are summarized in Tab. 5 together with the optimum conditions of the EDL. Note: the typical stabilization time required for the EDL at 52% and 400 mA was ca. 90 min. It should be highlighted that it is not just the highest SNR that needs to be considered for the choice of the optimum conditions but it is equally important to observe the day-to-day behaviour of the lamps, i.e., repeatability of their emission intensity. Therefore, the final optimum conditions are a compromise of their performance during each experiment and also of their overall endurance.

Tab. 5 Optimum operating conditions of the excitation sources employed in AFS

	EDL	**Superlamp**
Frequency (Hz)	40	40
Duty cycle (%)	52	28
Feeding current (mA)	400	18
Boost current (mA)	-	12

Furthermore, the intensity of the radiation emitted from the lamps was assessed using an optical power metre with a photodiode sensor at 307 nm lines (details in Appendix III). A comparison of the radiation intensities of the lamps operated under optimum conditions is given in Tab. 6. The line “Intensity” shows the time averaged radiation intensity whereas the line “Effective intensity” stands for the effective radiation intensity, i.e., the intensity during the time interval of the modulation period when the lamp is on. Tab. 6 also includes relevant parameters for both lamps such as sensitivity, peak height, SD_{blank} and $SD_{baseline}$. For a comprehensive comparison, relevant parameters were determined for the Superlamp with a duty cycle of 52%, matching EDL's optimal duty cycle. Primary and boost currents were optimized for this duty cycle using the same procedure as described above for the 28% duty cycle, refer to Tab. 6 for results. Notably, the data in Tab. 6 show that SD_{blank} is close to the same in all columns suggesting that blanks are not controlled either by contamination or by individual

sensitivities. Further, the reasonably good correlation between SD_{blank} and $SD_{baseline}$ indicates that the above discussed approach to optimization based on SNR is well grounded. However, the proportionality between the effective lamp radiation intensity and measured sensitivity is not absolutely direct, which may be caused by the fact that the sensitivities and the lamp radiation intensities were measured at different wavelengths, i.e., at 223 nm and 307 nm, respectively.

Tab. 6 Analytical parameters of Bi determination by HG-AFS with atomization in MDF atomizer using EDL and Superlamp and their radiation intensities

	EDL	**Superlamp**	
Duty cycle (%)	52	28	52
Feeding current (mA)	400	18[a]; 12[b]	12[a]; 10[b]
Intensity[c] (µW)	5.9 ± 1.1	1.1 ± 0.2	0.88 ± 0.18
Effective intensity[c] (µW)	11.3 ± 2.1	3.9 ± 0.7	1.7 ± 0.3
Sensitivity (µV s ng^{-1})	160 ± 23	15 ± 4	9.9 ± 0.2
Peak height (µV ng^{-1})	9.7 ± 0.8	0.8 ± 0.2	0.5 ± 0.1
SD_{blank} (µV s)	0.079 ± 0.005	0.05 ± 0.01	0.06 ± 0.01
$SD_{baseline}$ (µV)	0.055 ± 0.008	0.049 ± 0.005	0.04 ± 0.01
SNR[d]	175 ± 30	17 ± 4	13 ± 4
LOD (pg)	1.5	11	18

[a] primary current, [b] boost current, [c] measured with 307.1 nm interference filter, [d] related to 1 ng of Bi

3.1.4 Analytical characteristics of different approaches to Bi determination with AFS detection

Analytical figures of merit of Bi determination were evaluated for the two methodologies - HG-AFS and PVG-AFS. In the case of HG-AFS, the best results were achieved using the EDL (Tab. 6) and FIGS as the atomizer that was also chosen for atomization using PVG-AFS, typically providing around 1.7–1.8 higher sensitivity and SNR than MDF.

For HG-AFS using FIGS atomizer, the calibration functions constructed with 0, 0.04, 0.1, 0.25 and 1 μg L^{-1} Bi standard solutions were linear ($R^2 > 0.9999$) in the studied range. Furthermore, an outstanding repeatability <1% was achieved, expressed as the relative standard deviation (n = 10), at 1 μg L^{-1} Bi level. An extremely low LOD (3σ, n = 10) of 0.9 ng L^{-1} (0.9 pg absolute) was achieved.

For PVG-AFS using FIGS atomizer, the calibration function constructed with 0, 0.1, 0.25, 0.5, 1 and 2 μg L^{-1} Bi standard solutions was linear ($R^2 = 0.9998$). The repeatability, expressed as the relative standard deviation (n = 10), was 4% at 1 μg L^{-1}. The LODs achieved with PVG-AFS were found to be impaired by Bi contamination in the reaction medium and/or in the sensitizer. A distinctive peak shaped blank appeared over the recorded baseline. This phenomenon occurred due to the formation of $Bi(CH_3)_3$ vapours, which could only be produced within the injected sample/blank zone where Co^{2+} is present as the sensitizer as PVG cannot be accomplished from the photochemical medium without the sensitizer. Using FI-PVG-ICPMS, Bi concentration corresponding to this peak was estimated to be approximately 20 ng L^{-1} when the reaction medium was prepared from non-distilled acids and deionized water and it was then lowered to less than 10 ng L^{-1} when the acids, as well as deionized water, were purified by a sub-boiling distillation. Hence, a significant portion of the blank may originate from the added Co(II) acetate. Changing the supplier of Co(II) acetate did not further reduce Bi contamination. The lowest relative and absolute LOD (3σ, n = 10) achieved with PVG-AFS using purified acids and deionized water (DIW) corresponded to 12 ng L^{-1} and 6.7 pg, respectively.

The absolute LOD achieved with PVG-AFS is thus ca. 8 times higher than with HG-AFS, which can be attributed to several aspects. Firstly, the generation efficiency for PVG was estimated to be approximately 54% while more than 90% is expected for HG. Next, the measured peaks exhibited a FWHM approximately twice as large, which required extended integration times for evaluation. Lastly, the SD_{blank} was affected by contamination, as mentioned above.

3.1.5 Validation and application to real samples

To verify the accuracy and the practical feasibility, the proposed methodologies were applied to Bi determination in SRM of water 1643f (Trace Elements in Water). Furthermore, the HG-AFS methodology was further verified by Bi determination in seawater, blood, and hair

RMs. The determination was performed under optimum conditions of atomization in FIGS atomizer (Tab. 3 and 4) and with the 307 nm filter.

3.1.5.1 HG-AFS

The Bi content was quantified using the external calibration curve and recovery values were calculated from the slopes obtained with the standard addition technique (two spiked concentrations of standard to one replicate of each sample) related to the slope of the external calibration. Employing HG-AFS, the SRM 1643f was diluted approximately 80-fold with 1 mol L^{-1} HCl and analysed. The result 12.8 ± 0.1 μg L^{-1} is in a good agreement with the certified value, as can be seen in Tab. 7. The practical feasibility of the developed ultra-sensitive HG-AFS methodology was demonstrated on the analysis of seawater CASS-6 and NASS-7 materials, for which there weren't any certified/informative values available nor have there been any data provided in the literature yet. Bismuth concentration in seawater is typically very low (although there is a significant dispersion in the published data [11]), approximately 10–20 ng L^{-1} [103-105]. Minimal dilution of seawater CRMs is thus advised. The determined concentrations of 22 and 24 ng L^{-1} Bi (Tab. 7) are in accordance with the expected range and the spiked recovery in the range 89–100% further proved the suitability of the developed HG-AFS methodology for samples with matrices as complex as seawater without the necessity of a significant dilution.

The methodology was also verified using blood (Seronorm 1406264 Whole Blood L-2) and hair (GBW07601a Human hair) samples that required microwave digestion with nitric acid prior to the determination. The potential impact of residual nitric acid on the determination was examined and no interference was observed within the concentration range of 0.1–4 mol L^{-1}. The results of Bi determination by HG-AFS in the abovementioned samples are summarized in Tab. 7, showing excellent agreement with the certified value for the human hair material while the result for the blood RM falls within the certified concentration range.

Tab. 7 The determined content of Bi in certified reference materials, presented as median value (n = 3) ± SD, and spiked recoveries measured with HG-AFS

CRM	Certified value ($\mu g\ L^{-1}$)	Value obtained ($\mu g\ L^{-1}$)	Recovery[a] (%)
Fresh water 1643f	12.62 ± 0.11	12.8 ± 0.1	102 ± 1
Nearshore seawater CASS-6	-	0.024 ± 0.003	89 ± 3
Seawater NASS-7	-	0.022 ± 0.001	100 ± 3
Seronorm Whole Blood L-2	5 ± 1.01	6.2 ± 0.2	105 ± 1
GBW07601a Human hair	21 ± 2	20.1 ± 0.6	99 ± 1

[a] Spiked recovery = slope of standard additions (no addition and two spiked concentrations to a sample)/slope of external calibration

3.1.5.2 PVG-AFS

In order to validate the PVG-AFS methodology, Bi content was determined in SRM 1643f as well. The SRM 1643f Trace Elements in Water is stabilized in 0.32 mol L^{-1} HNO_3, which represents a huge obstacle to the determination by PVG-AFS since a severe interference from nitric acid occurs at >1 mmol L^{-1} (Appendix II). Unfortunately, there is no universal and always effective solution that would negate these interferences [106, 107] and appropriate sample dilution or evaporation to dryness with subsequent re-dissolving in the photochemical medium is usually employed.

In this study, an evaporation to dryness and subsequent dissolving with the photochemical medium (containing Co^{2+} as the sensitizer) was applied to SRM 1643f prior to analysis. The Bi content was quantified using the standard addition technique calibration curve and recovery values were calculated from the slopes obtained with the standard addition technique (two spiked concentrations of Bi standard to a sample) related to the slope of the external calibration curve. The determined content of 12.1 ± 0.9 μg L^{-1} is in good agreement with the certified value 12.62 ± 0.11 μg L^{-1} and the recovery of 97 ± 5% suggests efficient

removal of HNO_3 by evaporation, thus enabling fit-for-purpose quantification even using external calibration.

3.1.6 Conclusion

Different methodologies for Bi determination were successfully developed using the non-dispersive AFS: two based on HG-AFS, but using different excitation sources (EDL and Superlamp) and one based on PVG-AFS.

Firstly, HG was coupled with AFS and the atomization in MDF and FIGS atomizers was investigated in great detail. The FIGS atomizer offers a distinct advantage by enabling the Bi fluorescence measurement at lines around 307 nm that are typically overlapped by OH emission bands associated with the standard MDF atomizer. The remarkably low LOD at the ng L^{-1} level achieved with HG-AFS without any preconcentration step is primarily attributed to the high-intensity of the EDL used for excitation. The subsequent experiments dealing with the coupling of PVG to AFS suggest that the performance of MDF is independent of the generation technique (HG vs. PVG), however, the conditions of atomization in FIGS need to be adapted for PVG (increase of the O_2 supply) due to the presence of organic acid vapours released from the generator. The AFS instrument was also modified to enable the operation of the Superlamp as the excitation source in addition to the EDL. The radiation intensity of the EDL was proven to be significantly higher and proportionally reflected in the higher fluorescence intensity measured, thus also in higher sensitivity and lower LOD.

The developed methodologies were successfully validated for Bi determination in various sample matrices. It is especially worth mentioning that the HG-AFS methodology was found suitable for Bi determination in samples with matrices as complex as seawater. Normally, such a high concentration of salts in seawater is known to be an obstacle and a significant dilution is required prior to analysis by solution nebulization ICPMS.

3.2 Chemical vapour generation of Cd coupled to atomic fluorescence spectrometry for ultra-sensitive determination (Appendix IV)

The following section follows the paper by Sagapova et al. [53], where the authors compared the performances of CVG systems of Cd employing various modifiers (Co^{2+} ions/ascorbic acid/thiourea, Ti^{3+} or Ti^{4+}/KCN, and Cr^{3+}/KCN). The best results in terms of CVG efficiency, inter-day repeatability, and robustness were obtained with a four-channel system

employing Cr^{3+}/KCN as modifiers. In this work, this generator was coupled to AFS, the atomization in two flame atomizers was optimized, the analytical figures of merit assessed, and the methodology was validated by Cd determination in CRMs and rice samples.

3.2.1 *Initial assessment*

The AFS instrument developed at our laboratory excels in sensitivity thanks to the use of an intensive excitation source, the EDL, which results in extremely low LODs achieved for total As recently [71, 72] and also for Bi determination as demonstrated in subsection 3.1.4. Cadmium has even more potential when compared to the analytes mentioned above thanks to the special suitability of Cd for AFS detection [86, 108]. The resulting analytical performance might be limited by the CVG efficiency and background intensity. The former can be ruled out as the CVG efficiency was quantified in the range of 55–66% by Sagapova et al. [53]. The latter depends on several factors: the contamination of reagents by Cd, the scattered radiation from the EDL on the top of the atomizer and the flame emission. The flame emission in the employed wavelength range of 228 ± 10 nm was proven negligible for both MDF and FIGS by measuring signals with and without an ignited flame. In fact, preliminary experiments with FI-CVG-AFS revealed that there was a severe Cd contamination in the reagents, especially the deionized water and the modifier solutions of Cr^{3+} and KCN, which contributed to the increased background level. The concentrations of the modifiers used for the CVG were re-optimized and subsequently it was found that a decrease in the concentration of KCN in the modifier 2 (see Fig. 4) from 0.1 mol L^{-1} to 0.01 mol L^{-1} resulted in ca. 4 times lower background level. Importantly, the sensitivity and thus CVG efficiency remained unchanged. Moreover, this represents a great improvement compared to other papers in which 10–16 times higher concentrations of this highly toxic compound were necessary for efficient CVG of Cd [47-49, 53]. The concentrations of other reagents remained unchanged from the ones found optimal in Reference [53].

The optical path of the spectrometer (mutual distances of the three main components) was optimized so as to reach the highest peak area sensitivity and SNR, the same way as described in subsection 3.1.1. The optimal setting resulted in the radius of the radiation beam (circular) above the atomizer unit of approximately 5 mm. The power supply of the EDL was optimized in the range of 220–260 mA, the optimum was selected as 240 mA, which is also the recommended value.

3.2.2 Optimization of atomization conditions

The atomization conditions in the MDF and FIGS atomizers were optimized and the parameters were the total gas flow rate, the H_2 fraction, and observation height for both atomizers. In addition, the O_2 flow rate through the capillary was also optimized for the FIGS atomizer.

Firstly, the H_2 fraction of the gas phase entering the atomizer was optimized at a constant total gas flow rate of 400 and 500 mL min^{-1} for MDF and FIGS, respectively (Fig. 15). The fraction was optimized in the range from 17% to 50% for MDF and from 11% to 25% for FIGS. The lower the H_2 fraction, the higher the sensitivity, as well SNR, for both atomizers. Therefore, the H_2 fractions of 17% and 13% were selected as optimal for MDF and FIGS, respectively. It was impossible to operate the atomizers (long-term) at lower H_2 fraction as the flame would be extinguished by any small flow rate fluctuation, for example, when the reagents flows to the generator were stopped.

A similar optimization was carried out using MDF but without the ignition of the flame. At a 17% H_2 fraction, the sensitivity reached ca. 65% of the sensitivity obtained with the ignited flame and it even reached ca. 97% when only Ar_{flame} and $H_{2\ generator}$ (corresponding to 5% fraction) were employed (Fig. 15a). These results clearly indicated that a rather significant fraction of Cd volatile species entering the atomizer is in the form of free Cd atoms while the rest is molecular (most probably CdH_2), which is in agreement with previous results [53]. It should be noted that the sensitivities reached with and without ignited flames do not truly correspond to 65% fraction of free Cd atoms, because other factors need to be considered, such as the temperature distribution in the ignited flame and the fact that the free atoms are not shielded from the ambient atmosphere if no flame is maintained. Also, the repeatability is much worse without the flame and so is the background level - almost 4 times higher, as shown in Fig. 15b. That spoils the possibility of using the setup without the ignited flame as it would result in a poorer LOD.

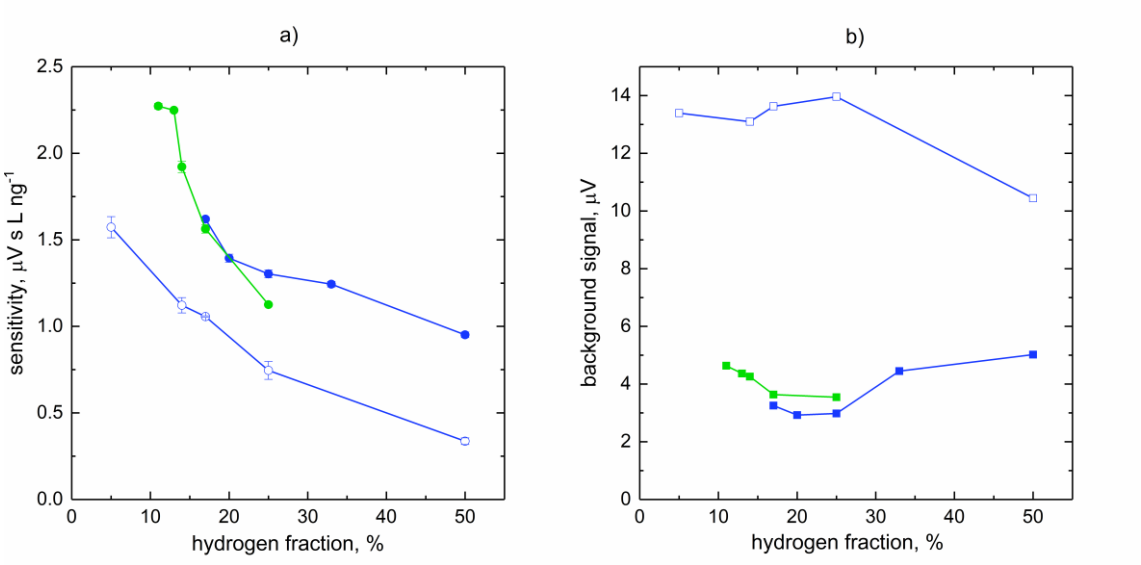

Fig. 15 The effect of the H_2 fraction on sensitivity (a) and background signal (b) measured with MDF (blue), with flame ignition (full) and without flame ignition (empty), and in FIGS (green); conditions: 250 ng L^{-1} Cd taken for CVG when the flames were ignited while 500 ng L^{-1} Cd taken for CVG for measurements without the ignited flame. Total gas flow rate corresponded to 400 and 500 mL min^{-1} for MDF and FIGS, respectively. SDs shown as error bars are indiscernible from the points in some cases.

Secondly, the total gas flow rate and the observation height were optimized at constant optimum H_2 fractions of 17% and 13% for MDF and FIGS, respectively (Fig. 16 and Fig. 17). The peak area and SNR were measured at various observation heights for total gas flow rate from 400 to 700 mL min^{-1}, 400 mL min^{-1} being the lowest applicable for both atomizers. Normally, the signal decreases with higher flow rates, which can be attributed to the dilution of free atoms in the observed volume of the flame. There was a prominent scattering of the radiation from the EDL at lower observation heights. The sufficient observation height at which there is no significant scattering on top of the atomizer unit corresponds to ≥7 mm for MDF and ≥5 mm for FIGS. The total gas flow rate of 400 mL min^{-1} was selected as optimum for both atomizers with observation height at 7 and 6 mm for MDF and FIGS, respectively. The optimum value is a compromise between the sensitivity, SNR, and the undesirable contribution of the scattered radiation to the background signal.

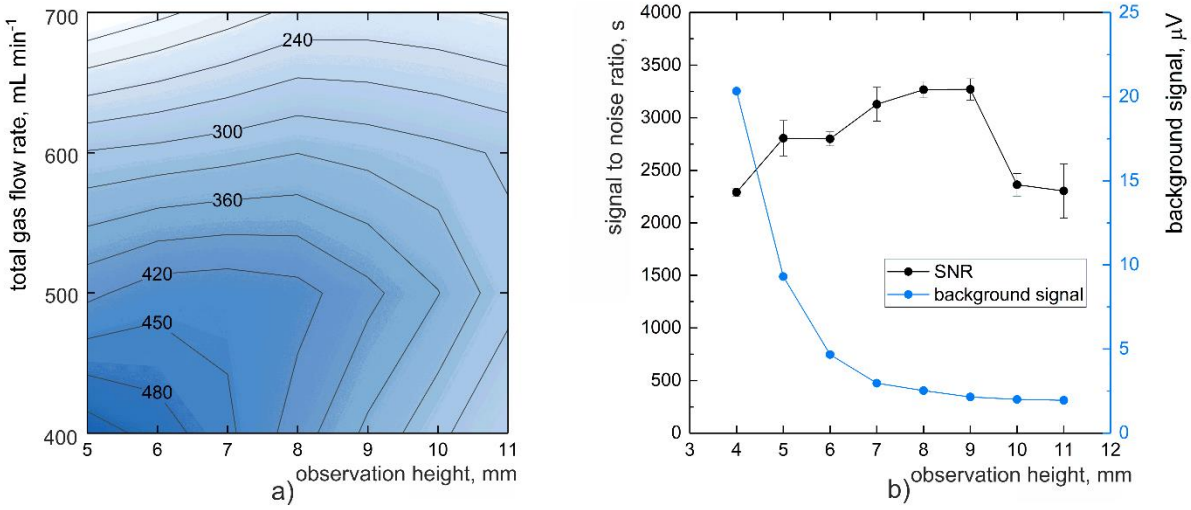

Fig. 16 The dependence of peak area (in µV s) on the total gas flow rate and observation height a) and the effect of the observation height on the SNR (black) and background signal (blue) at an optimum total gas flow rate of 400 mL min^{-1} (b) for MDF, both measured at a 17% H_2 fraction using 250 ng L^{-1} Cd for CVG.

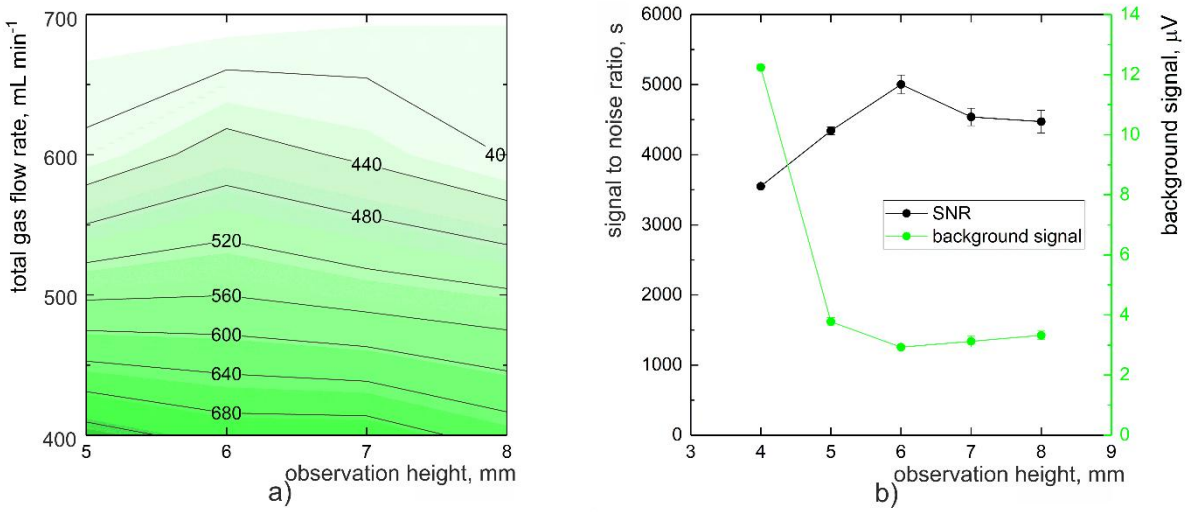

Fig. 17 The dependence of peak area (in µV s) on the total gas flow rate and observation height (a) and the effect of the observation height on the SNR (black) and background signal (green) at an optimum total gas flow rate 400 mL min^{-1} (b) for FIGS, both measured at a 13% H_2 fraction using 250 ng L^{-1} Cd for CVG.

Lastly, the O_2 flow rate through the capillary placed in the vertical axis of the support tube of FIGS was optimized. The flow rate was optimized in the range of 5–15 mL min^{-1} and a clear plateau of sensitivity appeared between 7 and 12 mL min^{-1} with an insignificant maximum at 12 mL min^{-1}. The background signal was however significantly lower, and therefore SNR higher, at flow rates higher than 10 mL min^{-1}. Lower O_2 flow rates are probably not sufficient

for the formation of H radicals and subsequent atomization of the fraction of molecular Cd species. Taking all that into consideration, the flow rate of 12 mL min^{-1} was selected as optimum. The shielding Ar flow rates were not optimized, the values from subsubsection 3.1.2.1 were used as the change of this parameter showed little to no influence on the analytical signal of Bi. The optimum atomization conditions for Cd volatile species are summarized in Tab. 8.

Tab. 8 Optimum atomization conditions of Cd for both flame atomizers

	Total Ar (mL min^{-1})	**Total H_2 (mL min^{-1})**	**O_2 (mL min^{-1})**	**$Ar_{shield\ I}$; $Ar_{shield\ II}$ (L min^{-1})**	**Observation height (mm)**
MDF	335	65	-	-	7
FIGS	345	55	12	1.5, 1.5	6

3.2.3 Analytical figures of merit

Analytical characteristics of the developed CVG-AFS methodology for Cd determination were evaluated and compared under optimal conditions for MDF and FIGS atomizers. The sensitivities and LODs were calculated from the calibration curves and blanks (n = 12). The calibration curves were linear ($R^2 > 0.9995$) in the measured concentration ranges, 0–350 ng L^{-1} for MDF and 0–250 ng L^{-1} for FIGS. The LODs corresponded to 1.40 ng L^{-1} and 0.42 ng L^{-1} for the MDF and FIGS, respectively, and the sensitivity achieved with FIGS was approximately 1.8 times higher than with MDF, which is also the reason for the lower LOD. To the best of our knowledge, the achieved LODs are the best reported for Cd determination using any VG based methodology without the need of a preconcentration step yet (see Tab. 4 in Appendix IV). Furthermore, an instrumental LOD, illustrating the fundamental potential and/or limitations of this methodology, was assessed. For this evaluation, the generator was supplied with only water through all the channels, the flame was ignited and operated under optimum conditions, and only blanks measured. Employing the values of sensitivity for the standard operation of the generator (with a supply of all the reagents), the resulting LODs corresponded to 0.3 ng L^{-1} and 0.1 ng L^{-1} for MDF and FIGS, respectively. The difference between the real and the instrumental LODs can be explained by either contamination of the employed reagents or the scattering of the radiation on the particles in the observation volume of the flame, or possibly both. The solid particles may be formed by vaporization in the flames

from the ballast aerosol droplets transported to the flame as a result of the fairly intense acid/$NaBH_4$ reaction. This is in an agreement with the observation of higher background signal detected when the flame was not ignited (cf. Fig. 15b), likely due to the presence of larger particles or insufficiently dried droplets.

3.2.4 Validation and application to real samples

The FIGS atomizer was selected for the validation of the developed CVG-AFS methodology thanks to its better analytical figures of merit. Cadmium content was determined in several CRMs of water with different levels of matrix complexity, and in CRM of rice as well as real samples of rice after microwave digestion in diluted acid medium. The details concerning the sample preparation scenario can be found in Appendix IV.

Firstly, the accuracy was verified by Cd determination in several water RMs: SRM 1643f (fresh water), ERM-CA713 (wastewater), NASS-5 (nearshore seawater), and CASS-4 (seawater). The SRM 1643f and ERM-CA713 were diluted 25 and 30-fold, respectively, with 0.2M HCl to fit inside the range of the external calibration curve (0–250 ng L^{-1}). The certified Cd content in the two seawater reference materials is around 25 ng L^{-1} which, taking the LOQ of 1.4 ng L^{-1} into consideration, leaves almost no room for any dilution. Therefore, the seawater CRMs were spiked with concentrated HCl just as to reach 0.2 M HCl in the final solution. The results are summarized in Tab. 9, which shows that the results are in a very good agreement with the certified values, even for the two CRMs of seawater analysed with essentially no dilution. On top of that, the recovery for NASS-5, examined by comparing the slope of the standard addition calibration (spiked concentrations of 50 and 150 ng L^{-1} Cd) and the slope of the external calibration, exhibited an excellent value of 101 ± 4%, which proved that there is no undesirable matrix effect from seawater on the determination of Cd by CVG-AFS. This is an important benefit of the developed methodology since the high salinity of this matrix normally requires considerable dilution prior to an analysis by conventional methods, e.g., using ICPMS with solution nebulization.

Tab. 9 Cd concentrations in water certified reference materials determined by CVG-AFS using FIGS atomizer; presented as median values ± SD (n = 3).

Samples	Cd concentration (μg L^{-1})	
	Determined	**Certified**
Fresh water 1643f	5.98 ± 0.44	5.89 ± 0.13
Wastewater ERM-CA713	4.95 ± 0.07	5.09 ± 0.2
Nearshore seawater CASS-4	0.025 ± 0.001	0.026 ± 0.003
Seawater NASS-5	0.020 ± 0.001	0.023 ± 0.003

Furthermore, the practical application was examined by Cd determination in three store-bought rice/rice flour products and SRM 1568b (rice flour), which required a more complicated sample preparation. Typically, the medium used for microwave digestion consists of concentrated HNO_3 and H_2O_2. However, concentrations higher than 0.3 mol L^{-1} of HNO_3 in the sample digests exhibited interference. To be more specific, a peak shaped blank appeared in the presence of 0.3 mol L^{-1} HNO_3 in the standard, corresponding to ca. 50 ng L^{-1} of Cd and the blank corrected sensitivity increased only slightly by 13%. In addition, the long-term performance of the CVG system was disrupted and the modification with 24 mmol L^{-1} Cr^{+3} solution had to be repeated to restore the original CVG efficiency. It was found that, in order to avoid any interfering effects from HNO_3, the samples need to be diluted so as to contain concentrations lower than 0.1 mol L^{-1} HNO_3. Thus, it was opted for 2 mol L^{-1} HNO_3 to be used for the microwave digestion so as to avoid significant dilution of the samples. Such concentration of HNO_3 was previously demonstrated to be efficient enough to complete microwave digestion [109].

The Cd content in all the samples was determined by CVG-AFS using the external calibration curve and the standard addition technique was applied to SRM 1568b to evaluate the recovery. Cadmium content was also quantified by conventional ICPMS with solution nebulization using an external calibration. There was a satisfactory agreement between the values obtained with both methodologies (Tab. 10). The results for the SRM 1568b were also in satisfactory agreement with the certified value of 22.4 ± 1.3 μg kg^{-1}. The recovery of the digest of SRM 1568b (calculated as the ratio of the slope of the standard addition to the slope of the external calibration) corresponded to 101 ± 2%, so no matrix effects were observed from this digest and the external calibration could be safely used for the determination. Hence, the

use of diluted HNO_3 for microwave digestion proved to be efficient, overcoming the potential interferences of higher concentrations of HNO_3 during CVG-AFS analyses. The highest concentration of Cd found in the real rice samples corresponded to 33.5 µg kg^{-1}, which is safely below the maximum limit established by the European Commission [110].

Tab. 10 Cd concentration in rice samples determined by CVG-AFS using FIGS atomizer and by conventional solution nebulization ICPMS; presented as median values ± SD (n = 3).

Samples	Cd concentration (µg kg^{-1})	
	FI-CVG-AFS	**Nebulization ICPMS**
Long grain rice (Vitana)	33.5 ± 0.5	32.2 ± 1.6
Rice flour (Paleta)	14.9 ± 0.9	14.1 ± 0.2
White rice flour (Cock brand)	9.0 ± 0.7	9.8 ± 0.2
SRM 1568b (rice flour)	19.9 ± 1.5	20.3 ± 1.1

3.2.5 Conclusion

A novel methodology for determination of ultra-trace concentrations of Cd using CVG coupled with non-dispersive AFS was developed.

The FIGS atomizer exhibited an overall better performance with the sensitivity almost twice as high as the sensitivity achieved with MDF, which is usually the standard atomizer used in AFS. An extremely low LOD of 0.42 ng L^{-1} achieved without any prior preconcentration step can be attributed especially to the high intensity of the EDL as well as high CVG efficiency. On the other hand, sensitivity so high brings additional issues to be dealt with - the impact of Cd contamination in the reagents on the background signal. This was partially solved by using only high purity reagents. The consumption of the KCN modifier was significantly reduced compared to other studies, however, it should be stated that the use of this modifier still poses health risks and proper waste handling is strongly advised.

It was demonstrated that this methodology is even suitable for direct determination (without any dilution) of low concentrations of Cd in complex samples such as seawater, i.e., samples with high salinity. A concentration of dissolved salts as high as in seawater is well known to be an obstacle for the conventional ICPMS with solution nebulization, which is recognized as the hallmark of unparalleled sensitivity, and it therefore requires significant

sample dilution prior to the determination. Furthermore, the methodology was validated for Cd determination in rice and rice flour samples after microwave digestion in a diluted acid medium.

3.3 Photochemical vapour generation of Ni coupled with atomic fluorescence spectrometry

In this part, the yet unpublished results achieved with PVG-AFS are described. The conditions for PVG of Ni using the thin-film flow-through photoreactor were taken over from Reference [70], where ICPMS was employed for the detection. The optimal photochemical medium composed of 30% (m/v) formic acid and the optimal flow rate through the photoreactor was 1.5 mL min^{-1}, which corresponds to an irradiation time of 29 s. PVG efficiency of 51 ± 2 % was determined by the previously described approach, by comparison of sensitivities obtained with ICPMS detection using solution nebulization and PVG [70, 111-113], hence, it was even better than the value of 42 ± 2 % described previously [70]. This discrepancy is likely due to the fact that a completely new thin-film flow-through photoreactor (Hg lamp) was employed for the purpose of this study. After coupling the PVG system with AFS, the atomization conditions in two flame atomizers were optimized, the analytical characteristics were assessed, and the precision of the method was verified by determination of Ni content in several water reference materials and real samples.

3.3.1 Coupling of PVG with AFS and initial assessment

The excitation source used for the excitation of Ni free atoms was the Superlamp since no EDL of Ni is commercially available. The operation of the Superlamps including the power source was previously thoroughly studied for Bi as described in subsection 3.1.3. However, the focusing of the radiation from the Ni Superlamp onto the volume of the flame had to be optimized again as well as were the lamp power supply. The distance between the lens on the rim of the lamp holder and the vertical axis of the atomizer was set to 48 mm. As it is evident from the measured emission spectrum of Ni HCL in Fig. 18, the most prominent Ni emission line is at 232.0 nm, which also corresponds to the strongest and most often used fluorescence line [114-116]. Therefore, the interference filter with central wavelength at 232.0 nm was selected, its transmission bandwidth of 10 nm is also shown in Fig. 18.

Regarding the power supply, the optimization went as follows. Firstly, the anode current was optimized without applying any boost current, i.e., operating the excitation source as a

standard HCL, at both 28% and 52% duty cycle (as taken over from subsection 3.1.3). Surprisingly, the "behaviour" of the Ni lamp differed from the Bi lamp significantly. The highest response was achieved with 19 mA primary current and 52% duty cycle while in the case of Bi, substantially better results were achieved when the lamp was operated at 28% duty cycle. The boost current for Ni Superlamp was optimized at three different values of the primary current: 11, 15, and 19 mA. It turned out that the higher the primary current, the higher the optimum boost current, which is a complete opposite to the results obtained for Bi. The optimum boost current for 11 and 15 mA primary current was 18 and 22 mA, respectively. The highest SNR was reached at 26 mA boost current for 19 mA primary current, however, the sensitivity kept increasing with even higher boost current values. As stated above, it is very important to consider both the analytical performance and the overall endurance of the lamp when choosing the optimum operating currents. Therefore, 19 mA anode current and 26 mA boost current (operated at 52% duty cycle) were chosen as optimum, both still in the recommended range by the manufacturer.

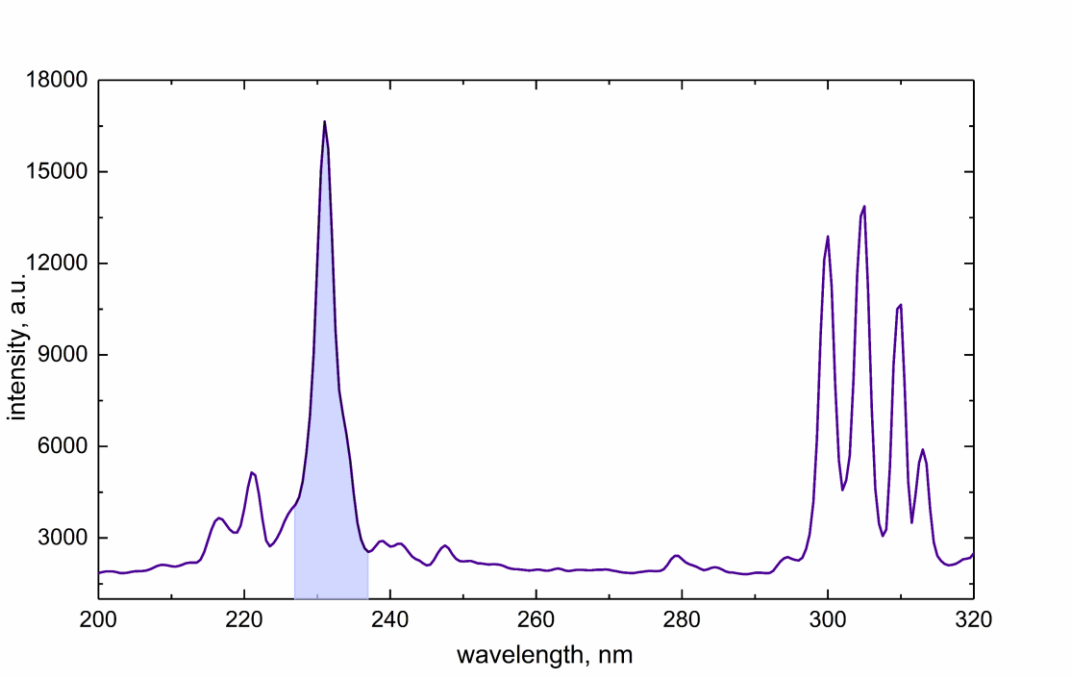

Fig. 18 Emission spectrum of Ni HCL (primary current 15 mA) obtained with a fibre optics UV-vis spectrometer. Transmission bandwidth (FWHM 10 nm) of 232 nm filter shown in colour for clarity.

3.3.2 Optimization of atomization conditions

The atomizers used for the atomization of Ni volatiles species were the same as in previous experiments for Bi and Cd - the MDF and FIGS atomizer. The default atomization conditions followed on from the optimum conditions for PVG-AFS of Bi, summarized in Tab. 4 in subsubsection 3.1.2.2. The main parameters to evaluate the results were the peak area (sensitivity) and the SNR. Firstly, the effect of H_2 fraction in MDF was optimized. The highest response as well SNR were obtained at 20% H_2 fraction (Fig. 19a). The peak area response rapidly decreased at 13% H_2 fraction, which was also the lowest fraction at which the flame was still somewhat stable.

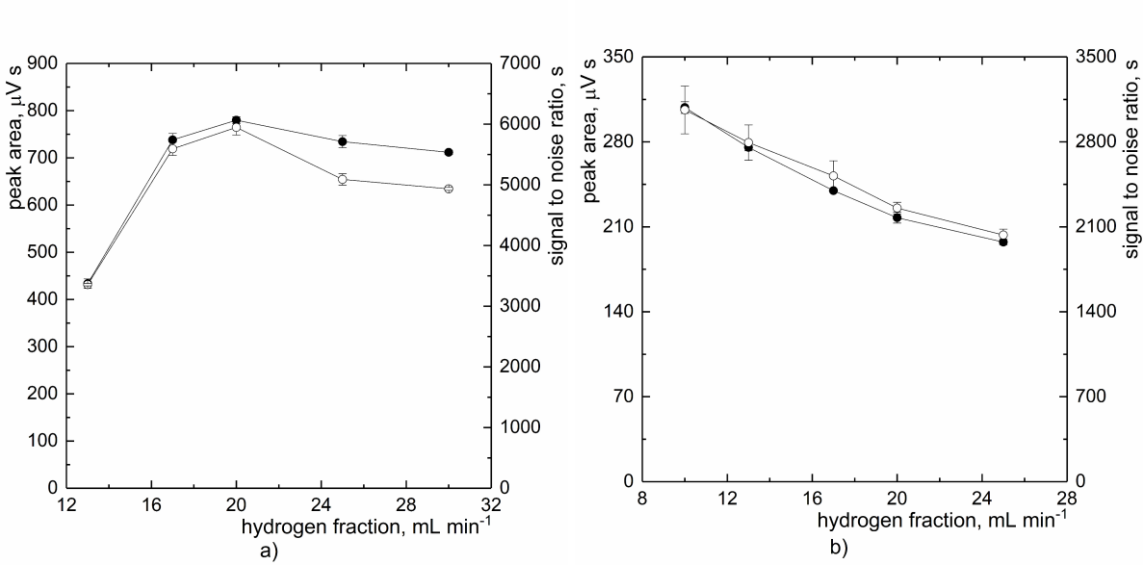

Fig. 19 Dependence of peak area (full circle) and SNR (empty circle) on hydrogen fraction in MDF (a) and FIGS (b); conditions for MDF: 5 µg L^{-1} Ni taken for PVG, observation height of 6 mm, 500 mL min total gas flow rate; conditions for FIGS: 2 µg L^{-1} Ni taken for PVG, observation height of 7 mm, 500 mL min total gas flow rate, 12 mL min^{-1} O_2 flow rate, 1.5 ($Ar_{shield\ I}$) and 1.5 L min ($Ar_{shield\ II}$) of shielding Ar.

Secondly, the total gas flow rate and observation height was optimized in MDF (Fig. 20a). The minimum applicable observation height with regards to SNR is 6 mm since the background level is too high at observation heights lower than that. The highest sensitivity was obtained at 500 mL min^{-1} and observation height of 6 mm. The same parameters were also optimized for FIGS. It is clear that the sensitivity is increasing with lower H_2 fractions in FIGS (Fig. 19b). Unfortunately, it is not possible to use a fraction lower than 10%, which was therefore selected to be the optimum. The optimum total gas flow rate using the FIGS atomizer (Fig. 20b) is coincidentally also 500 mL min^{-1}. The highest SNR at this flow rate was reached

at observation height of 7 mm, lower values resulted in an undesirably high background signal. Furthermore, the O_2 flow rate through the capillary was optimized, both the highest response and SNR were achieved with 15 mL min^{-1} with the signal significantly declining at 20 mL min^{-1} (Fig. 21). The flow rates of shielding Ar were not optimized again, they were merely taken over from subsubsection 3.1.2.1, where they were optimized for HG-AFS of Bi, as it showed little influence on the analytical response and SNR. The final optimum conditions for atomization of Ni are summarized in Tab. 11.

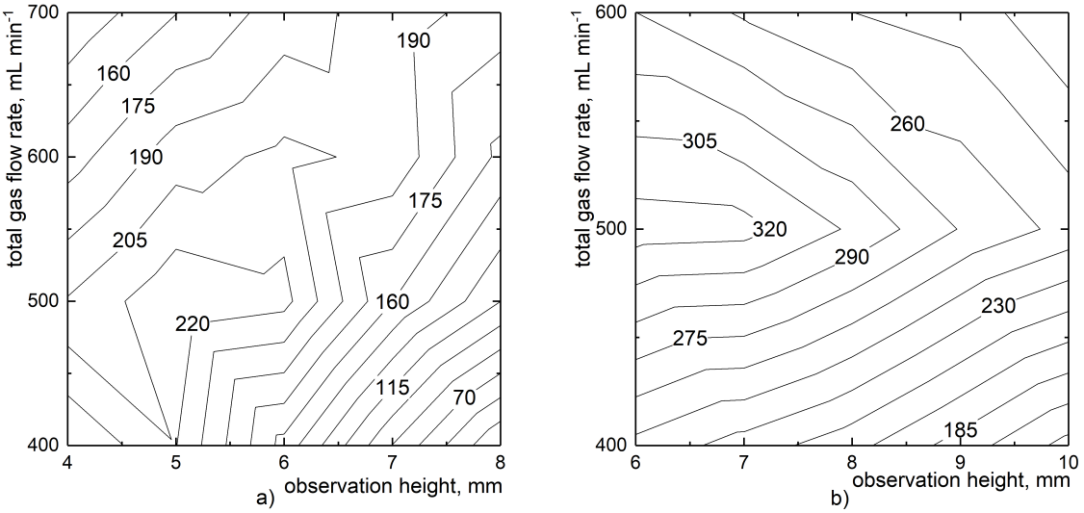

Fig. 20 Dependence of peak area (in µV s) on total gas flow rate and observation height in (a) MDF and (b) FIGS; conditions for MDF: 2 µg L^{-1} Ni taken for PVG, H_2 fraction 17%; conditions for FIGS: 2 µg L^{-1} Ni taken for PVG, H_2 fraction 10%, 12 mL min^{-1} O_2 flow rate, 1.5 ($Ar_{shield\ I}$) and 1.5 L min^{-1} ($Ar_{shield\ II}$) of shielding Ar. The observation height points measured were in the range of 4–8 (MDF) and 6–10 (FIGS) mm, by 1 mm. The total flow rate points measured were in the range of 400–600 (MDF) and 400–700 (FIGS) mL min^{-1}, by 100 mL min^{-1}.

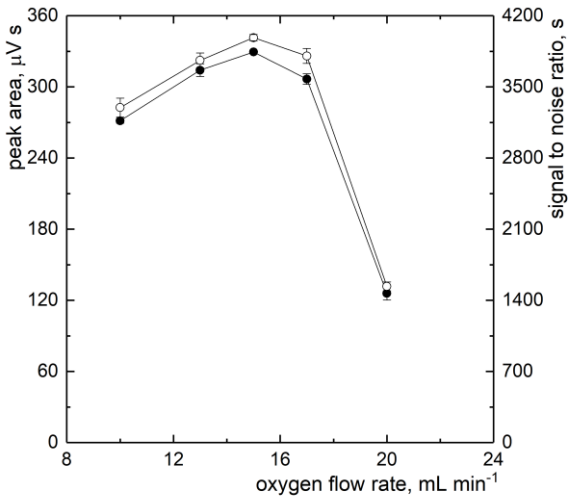

Fig. 21 Dependence of peak area (full circle) and SNR (empty circle) on O_2 flow rate in FIGS; conditions: 2 µg L^{-1} Ni taken for PVG, 500 mL min^{-1} total gas flow rate, H_2 fraction 10%, 1.5 ($Ar_{shield\ I}$) and 1.5 L min^{-1} ($Ar_{shield\ II}$) of shielding Ar, observation height of 6 mm.

Tab. 11 Optimum conditions of atomization of Ni in MDF and FIGS for PVG-AFS

	Ar (mL min^{-1})	**H_2 (mL min^{-1})**	**O_2 (mL min^{-1})**	**$Ar_{shield\ I}$; $Ar_{shield\ II}$ (L min^{-1})**	**Observation height (mm)**
MDF	400	100	-	-	6
FIGS	425	75	15	1.5; 1.5	7

3.3.3 Analytical figures of merit

The analytical characteristics of the newly developed methodology for Ni determination by PVG-AFS were assessed for both MDF and FIGS atomizers. Both calibration curves were constructed with standard solutions of 0, 50, 100, 400 and 2000 ng L^{-1} Ni and were linear in the whole range (R^2 = 0.9998 in both cases). The repeatability, expressed as the RSD (n = 10), at concentration level of 2 µg L Ni^{-1} corresponded to 2% in both cases. The achieved LODs were 7.9 and 5.3 ng L^{-1} for MDF and FIGS, respectively, and they are significantly better than those reported previously with various VG approaches coupled to AFS, see Tab. 12. The sensitivity achieved with FIGS is ca. 1.5 times higher than for MDF, which also corresponds to

the difference in LODs. The LOD value of 5.3 ng L^{-1} achieved with the FIGS atomizer is approximately 2.7 times higher than that achieved with PVG-ICPMS previously [70].

Tab. 12 Comparison of LODs for Ni determination based on AFS and various VG approaches reported in literature

Method	LOD (ng L^{-1})	VG details	Ref.
PVG-AFS	7.9[a]; 5.3[b]	thin-film flow-through photoreactor, 30% (m/v) formic acid as the photochemical medium, 29 s irradiation time	This work
PVG-AFS	10	heated quartz coiled photoreactor, 20% (v/v) formic acid as the photochemical medium, 120 s irradiation time	[117]
PVG-AFS	100	quartz coiled photoreactor, on-line mixing of sample in 2% (v/v) FA, 90% (v/v) FA, and 70% (v/v) NH_4OH (pH 2.95), 220 s irradiation time	[118]
CVG-AFS	650	KBH_4 reduction in the presence of sodium diethyldithiocarbamate and 1-butyl 3-methylimidazolium bromide	[119]
CVG-AFS	1000	KBH_4 reduction in the presence of ammonium pyrrolidine dithiocarbamate	[120]

[a] with MDF atomizer

[b] with FIGS atomizer

3.3.4 Validation

The developed methodology was verified by Ni determination in two water CRMs – SRM 1643f Trace Elements in Water and ERM-CA713 Wastewater. Both CRMs are stabilized in acid, namely SRM 1643f in 0.32 mol L^{-1} and ERM-CA713 in ca. 0.01 mol L^{-1} HNO_3. This can constitute a serious problem for direct Ni determination by PVG as demonstrated by Šoukal and Musil who found that even concentration of HNO_3 as low as 1 mmol L^{-1} suppresses the response of Ni by 10% [70]. With this in mind and respect to high concentrations of Ni in SRM 1643f and ERM-CA713, these materials were significantly diluted (100 times) and prepared in 30% (m/v) formic acid prior to PVG. The standard addition technique was employed for quantification by PVG-AFS. Furthermore, Ni content was determined in two real samples of well water. These sample were filtered (0.45 μm syringe filter) and approximately 10 times diluted to contain 30% (m/v) formic acid. The standard addition calibration technique was employed for quantification by PVG-AFS again. To obtain reference values, Ni content in well water samples was also determined by ICPMS with solution nebulization (Agilent 8900), using He collision cell mode and ^{60}Ni and ^{103}Rh (used as an internal standard) isotopes for evaluation. In this case, the water samples were prepared in 2% (m/v) HNO_3. The results obtained with the developed PVG-AFS methodology are in good agreement with the certified and reference values and they are summarized in Tab. 13.

Tab. 13 Ni concentrations in water certified reference materials and real well water samples determined by PVG-AFS using FIGS atomizer; presented as median values ± SD (n = 3).

Samples	Cd concentration (μg L^{-1})	
	Determined by PVG-AFS	**Certified/Reference[a]**
Fresh water 1643f	59.4 ± 1.6	59.8 ± 1.4
Wastewater ERM-CA713	50.5 ± 0.7	50.3 ± 1.4
Well water 1	4.4 ± 0.1	4.5 ± 0.1[a]
Well water 2	2.6 ± 0.1	2.7 ± 0.1[a]

[a] determined by ICPMS with solution nebulization

3.3.5 Conclusion

A thin-film flow-through photoreactor was successfully coupled to AFS for the determination of Ni. The volatile species of Ni – $Ni(CO)_4$ – was generated from 30% (m/v) formic acid used as the photochemical medium. The operational parameters of Ni Superlamp, which was used as the excitation source, were examined and the atomization process in MDF and FIGS atomizers was optimized. Around 1.5 times higher sensitivity and correspondingly lower LOD was achieved with FIGS than with MDF, hence, the FIGS was chosen as the atomizer for analytical application to several water (certified) reference materials. To overcome potential interfering effects of HNO_3, Ni content was successfully determined by PVG-AFS using the standard addition calibration technique and the obtained results were in good agreement with the (certified) reference values. As evident from Tab. 12, the lowest LOD for Ni determination by any VG approach coupled with AFS has been achieved here.

4 Concluding remarks

In this comprehensive study, the versatility of AFS was demonstrated by coupling it with various VG techniques for the sample introduction. Various methodologies were developed for the determination of Bi, Cd, and Ni. The common denominator of them all is the research-grade non-dispersive AFS constructed in a laboratory from easily available components - the excitation source, the atomizer, and the photomultiplier tube.

Firstly, the AFS was adapted for Bi determination employing HG for sample introduction and the EDL as the excitation source. The main efforts were directed to a detailed exploration of the atomization process in two hydride atomizers, namely MDF and FIGS, and to a subsequent comparison of the analytical performances achieved with them. The distinctive advantage of the FIGS atomizer is that it allows us to employ Bi fluorescence lines at >300 nm where serious OH emission can be an obstacle with the standard MDF atomizer. The exceptionally low LOD of 0.9 ng L^{-1} achieved with the FIGS and without any preconcentration step can be ascribed mainly to the high radiation intensity of the EDL in which, however, impurities of Sb and Hg were identified. Sb in particular caused serious positive interference on Bi determination with 202 nm and 223 nm interference filters. This challenge was effectively addressed by employing the 307 nm filter, where no Sb line is present. FIGS as the atomizer and the 307 nm filter were finally chosen to be suitable for Bi determination. Subsequently, the AFS instrument was modified to operate the Superlamp as the excitation source. The power supply of the Superlamp was optimized for Bi and the analytical performance was compared to that achieved with the EDL. The radiation intensity of the EDL was proven to be higher, as expected, and was proportionally reflected in the higher fluorescence intensity measured, thus also in higher sensitivity and lower LOD. To our best knowledge, such a direct comparison has not been made yet, since the currently available commercial or research-grade spectrometers usually allow the use of only one of them.

Furthermore, the spectrometer was coupled with PVG of Bi. Again, the atomization conditions in the MDF and FIGS were optimized and the optimum conditions differed only slightly from those obtained for HG-AFS. The most significant difference was the necessity for introduction of a higher O_2 flow rate to FIGS, most probably due to the presence of acetic and formic acid vapours employed for PVG. The absolute LOD obtained with PVG was around 8 times higher than with HG which can be attributed to lower PVG efficiency compared to that expected for HG, wider peaks, and the analyte contamination in blanks.

Among the main goals of this work was to adapt the spectrometer to the determination of transition metals, namely Cd and Ni. The developed methodology for Cd determination was based on special CVG system (assisted by Cr^{3+}/KCN modifiers) and the EDL as the excitation source for AFS. The FIGS atomizer outperformed the MDF atomizer, with sensitivity nearly double that of MDF. The extremely low LOD of 0.42 ng L^{-1}, achieved without resorting to preconcentration, is attributed to the high radiation intensity of the EDL again but also efficient CVG. However, the high sensitivity introduces some challenges, such as the serious impact of Cd contamination in the used reagents on the background signal, which has to be mitigated by using high-purity reagents. The methodology proved to be suitable even for direct determination of low Cd concentration in seawater samples, which is normally an obstacle faced by conventional ICPMS with solution nebulization. Additionally, the methodology was validated for Cd determination in rice and rice flour samples after microwave digestion in a diluted acid medium.

Last part of this thesis was dedicated to PVG of Ni from formic acid based medium and its coupling to AFS in order to demonstrate the applicability of AFS to wider range of elements. The Superlamp was used as the excitation source and the operational parameters were carefully optimized in order to reach the best analytical performance and maintain the lifetime of the lamp. Very high sensitivity and low LOD (around 5 ng L^{-1}) was finally achieved with the FIGS atomizer and this sensitive methodology was successfully verified by Ni determination in several water reference materials.

To conclude, the possibilities of a research-grade AFS were explored in a great detail. Most importantly, various VG techniques, such as HG, CVG, or PVG, can be coupled to the spectrometer and the applicability was further widened by the possibility of using two various types of excitation sources – EDL and the Superlamp. By achieving the interchangeability of the two excitation sources, it is possible to draw from the pros of both and partially eliminate the cons. Last but not least, all the developed methodologies described in this thesis were found suitable for ultra-sensitive determination of the analytes (Bi, Cd, and Ni) in various matrices and at a reasonable price point, especially when compared to other instrumentation normally used for ultra-trace element analysis.

5 References

[1] A. D. McNaught, A. Wilkinson: Compendium of chemical terminology, Blackwell Science Oxford, 1997.

[2] R. J. C. Brown, M. J. T. Milton: Analytical techniques for trace element analysis: an overview, TrAC Trends in Analytical Chemistry, 24 (2005) 266–274.

[3] E. Bulska, A. Ruszczyńska: Analytical Techniques for Trace Element Determination, Physical Sciences Reviews, 2 (2017) 20178002 .

[4] M. Nordberg, G. F. Nordberg: Trace element research-historical and future aspects, Journal of Trace Elements in Medicine and Biology, 38 (2016) 46–52.

[5] Z. L. He, X. E. Yang, P. J. Stoffella: Trace elements in agroecosystems and impacts on the environment, Journal of Trace Elements in Medicine and Biology, 19 (2005) 125–140.

[6] D. J. Swaine: Why trace elements are important, Fuel Processing Technology, 65–66 (2000) 21–33.

[7] N. Johri, G. Jacquillet, R. Unwin: Heavy metal poisoning: the effects of cadmium on the kidney, BioMetals, 23 (2010) 783–792.

[8] L. Järup, A. Åkesson: Current status of cadmium as an environmental health problem, Toxicology and Applied Pharmacology, 238 (2009) 201–208.

[9] J. M. Moulis, F. Thévenod: New perspectives in cadmium toxicity: an introduction, Biometals, 23 (2010) 763–768.

[10] H. Zhang, M. Reynolds: Cadmium exposure in living organisms: A short review, Science of The Total Environment, 678 (2019) 761–767.

[11] M. Filella: How reliable are environmental data on 'orphan' elements? The case of bismuth concentrations in surface waters, Journal of environmental monitoring, 12 (2010) 90–109.

[12] E. Denkhaus, K. Salnikow: Nickel essentiality, toxicity, and carcinogenicity, Critical Reviews in Oncology/Hematology, 42 (2002) 35–56.

[13] R. F. Browner, A. W. Boorn: Sample introduction: the Achilles' heel of atomic spectroscopy?, Analytical Chemistry, 56 (1984) 786–798.

[14] A. D'Ulivo, R. Sturgeon: Vapor Generation Techniques for Trace Element Analysis: Fundamental Aspects, Amsterdam, Elsevier Science, 2022.

[15] R. E. Russo, X. Mao, H. Liu, J. Gonzalez, S. S. Mao: Laser ablation in analytical chemistry—a review, Talanta, 57 (2002) 425–451.

[16] W. R. Hatch, W. L. Ott: Determination of submicrogram quantities of mercury by atomic absorption spectrophotometry, Analytical Chemistry, 40 (1968) 2085–2087.

[17] W. Holak: Gas-sampling technique for arsenic determination by atomic absorption spectrophotometry, Analytical Chemistry, 41 (1969) 1712–1713.
[18] R. E. Sturgeon, Z. Mester: Analytical Applications of Volatile Metal Derivatives, Applied Spectroscopy, 56 (2002) 202–213.
[19] J. Dědina, D.L. Tsalev: Hydride generation atomic absorption spectrometry, Wiley, 1995.
[20] R. S. Braman: Membrane probe-spectral emission type detection system for mercury in water, Analytical Chemistry, 43 (1971) 1462–1467.
[21] Y. L. Feng, R. E. Sturgeon, J. W. Lam: Generation of Atomic and Molecular Cadmium Species from Aqueous Media, Analytical Chemistry, 75 (2003) 635–640.
[22] W. B. Robbins, J. A. Caruso: Development of hydride generation methods for atomic spectroscopic analysis, Analytical Chemistry, 51 (1979) 889–898.
[23] A. D'Ulivo, J. Dědina, Z. Mester, R. E. Sturgeon, Q. Wang, B. Welz: Mechanisms of chemical generation of volatile hydrides for trace element determination (IUPAC Technical Report), Pure and Applied Chemistry, 83 (2011) 1283–1340.
[24] J. Dědina: Flow methods in gas-liquid separations, in: A. Sanz-Medel (Ed.) Flow Analysis with Atomic Spectrometric Detectors, Amsterdam, Elsevier Science, 1999, pp. 237–273.
[25] A. D'Ulivo, Z. Mester, R. E. Sturgeon: The mechanism of formation of volatile hydrides by tetrahydroborate(III) derivatization: A mass spectrometric study performed with deuterium labeled reagents, Spectrochimica Acta Part B: Atomic Spectroscopy, 60 (2005) 423–438.
[26] S. A. Pergantis, W. Winnik, E. M. Heithmar, W. R. Cullen: Investigation of arsine-generating reactions using deuterium-labeled reagents and mass spectrometry, Talanta, 44 (1997) 1941–1947.
[27] T. Freund: Anomalous hydrogen-deuterium distribution in stibine prepared from antimony(III) and borohydride in heavy water, Journal of the American Chemical Society, 83 (1961) 2779–2779.
[28] A. D'Ulivo, M. Onor, E. Pitzalis: Role of Hydroboron Intermediates in the Mechanism of Chemical Vapor Generation in Strongly Acidic Media, Analytical Chemistry, 76 (2004) 6342–6352.
[29] A. D'Ulivo: Mechanism of generation of volatile species by aqueous boranes: Towards the clarification of most controversial aspects, Spectrochimica Acta Part B: Atomic Spectroscopy, 65 (2010) 360–375.
[30] A. D'Ulivo, C. Baiocchi, E. Pitzalis, M. Onor, R. Zamboni: Chemical vapor generation for atomic spectrometry. A contribution to the comprehension of reaction mechanisms in the

generation of volatile hydrides using borane complexes, Spectrochimica Acta Part B: Atomic Spectroscopy, 59 (2004) 471–486.
[31] A. D'Ulivo: The contribution of chemical vapor generation coupled with atomic or mass spectrometry to the comprehension of the chemistry of aqueous boranes, Journal of Analytical Atomic Spectrometry, 34 (2019) 823–847.
[32] A. D'Ulivo: Mechanisms of chemical vapor generation by aqueous tetrahydridoborate. Recent developments toward the definition of a more general reaction model, Spectrochimica Acta Part B: Atomic Spectroscopy, 119 (2016) 91–107.
[33] P. Pohl: Recent advances in chemical vapour generation via reaction with sodium tetrahydroborate, TrAC Trends in Analytical Chemistry, 23 (2004) 21–27.
[34] T. Matoušek: The efficiency of chemical vapour generation of transition and noble metals, Analytical and Bioanalytical Chemistry, 388 (2007) 763–767.
[35] R. Sturgeon, J. Liu, V. Boyko, V. Luong: Determination of copper in environmental matrices following vapor generation, Analytical chemistry, 68 (1996) 1883–1887.
[36] P. Pohl, P. Jamroz, M. Welna, A. Szymczycha-Madeja, K. Greda: Chemical-vapor generation of transition metals through the reaction with tetrahydroborate in recent achievements in analytical atomic spectrometry, TrAC Trends in Analytical Chemistry, 59 (2014) 144–155.
[37] M. G. C. Fernandez, M. A. Palacios, C. Camara: Flow-injection and continuous-flow systems for the determination of Se(IV) and S (VI) by hydride generation atomic absorption spectrometry with on-line prereduction of Se(VI) to Se(IV), Analytica Chimica Acta, 283 (1993) 386–392.
[38] O. Aastroem: Flow injection analysis for the determination of bismuth by atomic absorption spectrometry with hydride generation, Analytical Chemistry, 54 (1982) 190–193.
[39] N. A. Kasa, D. S. Chormey, Ç. Büyükpınar, F. Turak, T. B. Budak, S. Bakırdere: Determination of cadmium at ultratrace levels by dispersive liquid-liquid microextraction and batch type hydride generation atomic absorption spectrometry, Microchemical Journal, 133 (2017) 144–148.
[40] A. D'Ulivo, S. S. T. Battistini, E. Pitzalis, R. Zamboni, Z. Mester, R. E. Sturgeon: Effect of additives on the chemical vapour generation of bismuthane by tetrahydroborate(III) derivatization, Analytical and Bioanalytical Chemistry, 388 (2007) 783–791.
[41] J. Kratzer, J. Dědina: In situ trapping of bismuthine in externally heated quartz tube atomizers for atomic absorption spectrometry, Journal of Analytical Atomic Spectrometry, 21 (2006) 208–210.

[42] D. S. Lee: Determination of bismuth in environmental samples by flameless atomic absorption spectrometry with hydride generation, Analytical Chemistry, 54 (1982) 1682–1686.
[43] P. Schramel, L. Q. Xu: Determination of arsenic, antimony, bismuth, selenium and tin in biological and environmental samples by continuous flow hydride generation ICP-AES without gas-liquid separator, Fresenius' Journal of Analytical Chemistry, 340 (1991) 41–47.
[44] T. Nakahara, K. Nakanishi, T. Wasa: Determination of trace concentrations of bismuth by inductively coupled plasma-atomic emission spectrometry with hydride generation, Spectrochimica Acta Part B: Atomic Spectroscopy, 42 (1987) 119–128.
[45] L. Lampugnani, C. Salvetti, D. L. Tsalev: Hydride generation atomic absorption spectrometry with different flow systems and in-atomizer trapping for determination of cadmium in water and urine—overview of existing data on cadmium vapour generation and evaluation of critical parameters, Talanta, 61 (2003) 683–698.
[46] E. Pitzalis, D. Angelini, M. C. Mascherpa, A. D'Ulivo: Insight into the mechanisms controlling the chemical vapor generation of cadmium, Journal of Analytical Atomic Spectrometry, 33 (2018) 2160–2171.
[47] V. Yilmaz, L. Rose, Z. Arslan, M. D. Little: On-line chemical vapour generation of cadmium in the presence of hexacyanochromate(III) for determination by inductively coupled plasma mass spectrometry (ICP-MS), Journal of Analytical Atomic Spectrometry, 27 (2012) 1895–1902.
[48] V. Yilmaz, Z. Arslan, L. Rose, M. D. Little: Cyanovanadate(III) complexes as novel additives for efficient generation of volatile cadmium species in complex samples prior to determinations by inductively coupled plasma mass spectrometry (ICP-MS), Talanta, 115 (2013) 681–687.
[49] Z. Arslan, V. Yilmaz, L. Rose: Efficient generation of volatile cadmium species using Ti(III) and Ti(IV) and application to determination of cadmium by cold vapor generation inductively coupled plasma mass spectrometry (CVG-ICP-MS), Microchemical Journal, 123 (2015) 170–178.
[50] M. Valdés-Hevia y Temprano, M. F. de la Campa, A. Sanz-Medel: Generation of volatile cadmium species with sodium tetrahydroborate from organized media: application to cadmium determination by inductively coupled plasma atomic emission spectrometry, Journal of Analytical Atomic Spectrometry, 8 (1993) 847–852.
[51] A. Sanz-Medel, M. Valdés-Hevia y Temprano, N. Bordel Garcia, M. Fernández de la Campa: Generation of cadmium atoms at room temperature using vesicles and its application

to cadmium determination by cold vapor atomic spectrometry, Analytical Chemistry, 67 (1995) 2216–2223.
[52] X. Yuan, L. Yang, S. Liu, H. Yang, Y. Tang, K. Huang, M. Zhang: An effective analytical system based on an ultraviolet atomizer for trace cadmium determination using atomic fluorescence spectrometry, Analytical Methods, 10 (2018) 4821–4826.
[53] L. Sagapova, S. Musil, B. Kodríková, M. Svoboda, J. Kratzer: Effect of additives on cadmium chemical vapor generation and reliable quantification of generation efficiency, Analytica Chimica Acta, 1168 (2021) 338601.
[54] D. Leonori, R. E. Sturgeon: A unified approach to mechanistic aspects of photochemical vapor generation, Journal of Analytical Atomic Spectrometry, 34 (2019) 636–654.
[55] E. Kikuchi, H. Sakamoto: Kinetics of the Reduction Reaction of Selenate Ions by TiO2 Photocatalyst, Journal of The Electrochemical Society, 147 (2000) 4589.
[56] X. Guo, R. E. Sturgeon, Z. Mester, G. J. Gardner: Vapor Generation by UV Irradiation for Sample Introduction with Atomic Spectrometry, Analytical Chemistry, 76 (2004) 2401–2405.
[57] L. Li, C. Jiang, J. Xiao, H. Luo, S. Zhang, Z. Zou, K. Huang: Applications of photochemical vapor generation-analytical atomic spectrometry for the speciation analysis of arsenic, mercury and selenium, Spectrochimica Acta Part B: Atomic Spectroscopy, (2022) 106579.
[58] J. Hu, C. Li, Y. Zhen, H. Chen, J. He, X. Hou: Current advances of chemical vapor generation in non-tetrahydroborate media for analytical atomic spectrometry, TrAC Trends in Analytical Chemistry, 155 (2022) 116677.
[59] R. E. Sturgeon: Photochemical vapor generation: a radical approach to analyte introduction for atomic spectrometry, Journal of Analytical Atomic Spectrometry, 32 (2017) 2319–2340.
[60] M. Rybínová, V. Červený, J. Hraníček, P. Rychlovský: UV-Photochemical Generation of Volatiles in Atomic Spectrometric Methods, Chemické listy, 109 (2015) 930–937.
[61] D. Qin, F. Gao, Z. Zhang, L. Zhao, J. Liu, J. Ye, J. Li, F. Zheng: Ultraviolet vapor generation atomic fluorescence spectrometric determination of mercury in natural water with enrichment by on-line solid phase extraction, Spectrochimica Acta Part B: Atomic Spectroscopy, 88 (2013) 10–14.
[62] C. Zheng, Q. Ma, L. Wu, X. Hou, R. E. Sturgeon: UV photochemical vapor generation–atomic fluorescence spectrometric determination of conventional hydride generation elements, Microchemical Journal, 95 (2010) 32–37.

[63] Y. Yu, Y. Jia, Z. Shi, Y. Chen, S. Ni, R. Wang, Y. Tang, Y. Gao: Enhanced Photochemical Vapor Generation for the Determination of Bismuth by Inductively Coupled Plasma Mass Spectrometry, Analytical Chemistry, 90 (2018) 13557–13563.
[64] Y. Zhen, Y. Yu, A. Zhang, Y. Gao: Matrix-assisted photochemical vapor generation for determination of trace bismuth in FeNi based alloy samples by inductively coupled plasma mass spectrometry, Microchemical Journal, 151 (2019) 104242.
[65] Y. Jia, Q. Mou, Y. Yu, Z. Shi, Y. Huang, S. Ni, R. Wang, Y. Gao: Reduction of Interferences Using Fe-Containing Metal–Organic Frameworks for Matrix Separation and Enhanced Photochemical Vapor Generation of Trace Bismuth, Analytical Chemistry, 91 (2019) 5217–5224.
[66] Y. Yu, Q. Zhao, H. Bao, Q. Mou, Z. Shi, Y. Chen, Y. Gao: Determination of Trace Bismuth in Environmental Waters by ICP-MS with Cobalt Ion-Assisted Photochemical Vapour Generation, Geostandards and Geoanalytical Research, 44 (2020) 617–627.
[67] X. Guo, R. E. Sturgeon, Z. Mester, G. Gardner: UV photosynthesis of nickel carbonyl, Applied Organometallic Chemistry, 18 (2004) 205–211.
[68] Y. Shen, C. Zheng, X. Jiang, X. Wu, X. Hou: Integration of hydride generation and photochemical vapor generation for multi-element analysis of traditional Chinese medicine by ICP-OES, Microchemical Journal, 123 (2015) 164–169.
[69] M. Li, Y. Deng, X. Jiang, X. Hou: UV photochemical vapor generation–nitrogen microwave induced plasma optical emission spectrometric determination of nickel, Journal of Analytical Atomic Spectrometry, 33 (2018) 1086–1091.
[70] J. Šoukal, S. Musil: Detailed evaluation of conditions of photochemical vapor generation for sensitive determination of nickel in water samples by ICP-MS detection, Microchemical Journal, 172 (2022) 106963.
[71] S. Musil, T. Matoušek, J. M. Currier, M. Stýblo, J. Dědina: Speciation analysis of arsenic by selective hydride generation-cryotrapping-atomic fluorescence spectrometry with flame-in-gas-shield atomizer: achieving extremely low detection limits with inexpensive instrumentation, Analytical Chemistry, 86 (2014) 10422–10428.
[72] K. Marschner, S. Musil, J. Dědina: Flame-in-gas-shield and miniature diffusion flame hydride atomizers for atomic fluorescence spectrometry: optimization and comparison, Spectrochimica Acta Part B: Atomic Spectroscopy, 109 (2015) 16–23.
[73] J. Dědina: Generation of Volatile Compounds for Analytical Atomic Spectroscopy, in: R.A. Meyers (Ed.) Encyclopedia of Analytical Chemistry, Supplementary Volumes S1-S3, Chichester, UK, John Wiley & Sons, Ltd, 2011, pp. 897–936.

[74] J. Dědina: Atomization of volatile compounds for atomic absorption and atomic fluorescence spectrometry: On the way towards the ideal atomizer, Spectrochimica Acta Part B: Atomic Spectroscopy, 62 (2007) 846–872.
[75] B. Welz, M. Melcher: Investigations on atomisation mechanisms of volatile hydride-forming elements in a heated quartz cell: Part 1. Gas-phase and surface effects; decomposition and atomisation of arsine, Analyst, 108 (1983) 213–224.
[76] J. Dědina: Quartz tube atomizers for hydride generation atomic absorption spectrometry: mechanism of selenium hydride atomization and fate of free atoms, Spectrochimica Acta Part B: Atomic Spectroscopy, 47 (1992) 689–700.
[77] J. Dědina, I. Rubeška: Hydride atomization in a cool hydrogen—oxygen flame burning in a quartz tube atomizer, Spectrochimica Acta Part B: Atomic Spectroscopy, 35 (1980) 119–128.
[78] W. T. Corns, P. B. Stockwell, L. Ebdon, S. J. Hill: Development of an atomic fluorescence spectrometer for the hydride-forming elements, Journal of Analytical Atomic Spectrometry, 8 (1993) 71–77.
[79] J. Dědina, A. D'Ulivo, L. Lampugnani, T. Matoušek, R. Zamboni: Selenium hydride atomization, fate of free atoms and spectroscopic temperature in miniature diffusion flame atomizer studied by atomic absorption spectrometry, Spectrochimica Acta Part B: Atomic Spectroscopy, 53 (1998) 1777–1790.
[80] J. Dědina, A. D'Ulivo: Argon shielded, highly fuel-rich, hydrogen–oxygen diffusion microflame—a new hydride atomizer, Spectrochimica Acta Part B: Atomic Spectroscopy, 52 (1997) 1737–1746.
[81] K. Marschner, Á. H. Pétursdóttir, P. Bücker, A. Raab, J. Feldmann, Z. Mester, T. Matoušek, S. Musil: Validation and inter-laboratory study of selective hydride generation for fast screening of inorganic arsenic in seafood, Analytica Chimica Acta, 1049 (2019) 20–28.
[82] K. Marschner, S. Musil, I. Mikšík, J. Dědina: Investigation of hydride generation from arsenosugars-Is it feasible for speciation analysis?, Analytica Chimica Acta, 1008 (2018) 8-17.
[83] K. Marschner, S. Musil, J. Dědina: Achieving 100% efficient postcolumn hydride generation for As speciation analysis by atomic fluorescence spectrometry, Analytical Chemistry, 88 (2016) 4041–4047.
[84] A. D'Ulivo, I. Paolicchi, M. Onor, R. Zamboni, L. Lampugnani: Flame-in-gas-shield miniature flame hydride atomizers for ultra trace element determination by chemical vapor generation atomic fluorescence spectrometry, Spectrochimica Acta Part B: Atomic Spectroscopy, 64 (2009) 48–55.

[85] J. D. Winefordner, T. J. Vickers: Atomic Fluorescence Spectroscopy as a Means of Chemical Analysis, Analytical Chemistry, 36 (1964) 161–165.
[86] V. Sychra, V. Svoboda, I. Rubeška: Atomic Fluorescence Spectroscopy, New York, Van Nostrand Reinhold Company, 1975.
[87] P. L. Larkins, R. M. Lowe, J. V. Sullivan, A. Walsh: The use of solar-blind photomultipliers in flame spectroscopy, Spectrochimica Acta Part B: Atomic Spectroscopy, 24 (1969) 187–190.
[88] A. D'Ulivo, P. Papoff, C. Festa: A simultaneous multielement non-dispersive atomic-fluorescence spectrometer using modulated sources and frequency discrimination of fluorescence signals, Talanta, 30 (1983) 907–913.
[89] P. D. Warr: Use of a filter in atomic-fluorescence spectroscopy, Talanta, 17 (1970) 543–548.
[90] J. O. Weide, M. L. Parsons: Use of pulsed hollow cathode lamps in atomic fluorescence flame spectrometry, Analytical Letters, 5 (1972) 363–365.
[91] J. V. Sullivan, A. Walsh: High intensity hollow-cathode lamps, Spectrochimica Acta, 21 (1965) 721–726.
[92] J. D. Winefordner, R. A. Staab: Determination of Zinc, Cadmium, and Mercury by Atomic Fluorescence Flame Spectormetry, Analytical Chemistry, 36 (1964) 165–168.
[93] R. M. Dagnall, K. C. Thompson, T. S. West: An investigation of some experimental parameters in atomic fluorescence spectrophotometry, Analytica Chimica Acta, 36 (1966) 269–271.
[94] J. Dawson, D. Ellis: Pulsed current operation of hollow cathode lamps to increase the intensity of resonance lines for atomic absorption spectroscopy, Spectrochimica Acta Part A: Molecular Spectroscopy, 23 (1967) 565–569.
[95] O. Menis, T. Rains: Determination of arsenic by atomic absorption spectrometry with an electrodeless discharge lamp as a source of radiation, Analytical Chemistry, 41 (1969) 952–954.
[96] A. K. Gilmutdinov, B. Radziuk, M. Sperling, B. Welz, K. Y. Nagulin: Spatial distribution of radiant intensity from primary sources for atomic absorption spectrometry. Part II: Electrodeless discharge lamps, Applied Spectroscopy, 50 (1996) 483–497.
[97] Electrodeless Discharge Lamps, PerkinElmer. http://www.perkinelmer.com/category/electrodeless-discharge-lamps (accessed 20. 10. 2023).
[98] Super Lamps, PHOTRON, http://www.photronlamp.com/collections/super-lamps (accessed 20. 10. 2023).

[99] S. Musil, J. Dědina: A sapphire tube atomizer for on-line atomization and in situ collection of bismuthine for atomic absorption spectrometry, Journal of Analytical Atomic Spectrometry, 28 (2013) 593–600.
[100] Photomultipliers, PerkinElmer, https://resources.perkinelmer.com/corporate/cms-resources/images/44-6570dts_photomultipliersmoleculardetectionanalytical (accessed 20.10.2023).
[101] J. Dědina: Atomic absorption coefficient of the Se 196 nm line—theoretical calculation and experimental evaluation, Spectrochimica Acta Part B: Atomic Spectroscopy, 46 (1991) 379–391.
[102] I. B. Karadjova, L. Lampugnani, J. Dědina, A. D'Ulivo, M. Onor, D. L. Tsalev: Organic solvents as interferents in arsenic determination by hydride generation atomic absorption spectrometry with flame atomization, Spectrochimica Acta Part B: Atomic Spectroscopy, 61 (2006) 525–531.
[103] Š. Komorsky-Lovrić: Direct determination of bismuth(III) in sea water by square-wave anodic stripping voltammetry at a glassy-carbon rotating-disk electrode, Analytica Chimica Acta, 204 (1988) 161–167.
[104] J. E. Portman, J. P. Riley: The determination of bismuth in sea and natural waters, Analytica Chimica Acta, 34 (1966) 201–210.
[105] T. R. Gilbert, D. N. Hume: Direct determination of bismuth and antimony in sea water by anodic stripping voltammetry, Analytica Chimica Acta, 65 (1973) 451–459.
[106] G. S. Lopes, R. E. Sturgeon, P. Grinberg, E. Pagliano: Evaluation of approaches to the abatement of nitrate interference with photochemical vapor generation, Journal of Analytical Atomic Spectrometry, 32 (2017) 2378–2390.
[107] A. Mollo, M. Knochen: Towards the abatement of nitrate interference on selenium determination by photochemical vapor generation, Spectrochimica Acta Part B: Atomic Spectroscopy, (2020) 105875.
[108] R. C. Elser, J. D. Winefordner: A Simple Monochromatorless Atomic Fluorescence Flame Spectrometer, Applied Spectroscopy, 25 (1971) 345–346.
[109] G. C. L. Araújo, M. H. Gonzalez, A. G. Ferreira, A. R. A. Nogueira, J. A. Nóbrega: Effect of acid concentration on closed-vessel microwave-assisted digestion of plant materials, Spectrochimica Acta Part B: Atomic Spectroscopy, 57 (2002) 2121–2132.
[110] Commission Regulation (EU) 2021/1323 Regulation (EC) No 1881/2006 as regards maximum levels of cadmium in certain foodstuffs.

[111] S. Musil, E. Jeníková, J. Vyhnanovský, R. E. Sturgeon: Highly Efficient Photochemical Vapor Generation for Sensitive Determination of Iridium by Inductively Coupled Plasma Mass Spectrometry, Analytical Chemistry, 95 (2023) 3694–3702.
[112] S. Musil, J. Vyhnanovský, R. E. Sturgeon: Ultrasensitive Detection of Ruthenium by Coupling Cobalt and Cadmium Ion-Assisted Photochemical Vapor Generation to Inductively Coupled Plasma Mass Spectrometry, Analytical Chemistry, 93 (2021) 16543–16551.
[113] J. Vyhnanovský, R. E. Sturgeon, S. Musil: Cadmium Assisted Photochemical Vapor Generation of Tungsten for Detection by Inductively Coupled Plasma Mass Spectrometry, Analytical Chemistry, 91 (2019) 13306–13312.
[114] J. Matoušek, V. Sychra: Atomic fluorescence study on iron, cobalt, and nickel, Analytical Chemistry, 41 (1969) 518–522.
[115] D. Armentrout: Determination of Nickel by Atomic Fluorescence Flame Spectrometry, Analytical Chemistry, 38 (1966) 1235–1237.
[116] P. Larkins: Non-dispersive systems in atomic fluorescence spectroscopy—I: A single-channel system employing a solar-blind detector and an air-acetylene flame, Spectrochimica Acta Part B: Atomic Spectroscopy, 26 (1971) 477–489.
[117] L. Liu, H. Deng, L. Wu, C. Zheng, X. Hou: UV-induced carbonyl generation with formic acid for sensitive determination of nickel by atomic fluorescence spectrometry, Talanta, 80 (2010) 1239–1244.
[118] Y. Wang, K. Xu, X. Jiang, X. Hou, C. Zheng: Dual-mode chemical vapor generation for simultaneous determination of hydride-forming and non-hydride-forming elements by atomic fluorescence spectrometry, Analyst, 139 (2014) 2538–2544.
[119] C. Zhang, Y. Li, P. Wu, X. P. Yan: Synergetic enhancement effect of ionic liquid and diethyldithiocarbamate on the chemical vapor generation of nickel for its atomic fluorescence spectrometric determination in biological samples, Analytica Chimica Acta, 652 (2009) 143–147.
[120] C. Zeng, Y. Jia, Y. I. Lee, X. Hou, L. Wu: Ultrasensitive determination of cobalt and nickel by atomic fluorescence spectrometry using APDC enhanced chemical vapor generation, Microchemical Journal, 104 (2012) 33–37.

List of appendices

Appendix I

B. ŠTÁDLEROVÁ, M. KOLROSOVÁ, J. DĚDINA, S. MUSIL: Atomic fluorescence spectrometry for ultrasensitive determination of bismuth based on hydride generation – the role of excitation source, interference filter and flame atomizers. Journal of Analytical Atomic Spectrometry, 35 (2020), 993–1002, DOI: 10.1039/d0ja00043d.

Appendix II

J. VYHNANOVSKÝ, D. YILDIZ, **B. ŠTÁDLEROVÁ**, S. MUSIL: Efficient photochemical vapor generation of bismuth using a coiled Teflon reactor: effect of metal sensitizers and analytical performance with flame-in-gas-shield atomizer and atomic fluorescence spectrometry. Microchemical Journal, 164 (2021), 105997, DOI: 10.1016/j.microc.2021.105997.

Appendix III

B. ŠTÁDLEROVÁ, J. DĚDINA, S. MUSIL: Comparison of bismuth atomic lamps for a non-dispersive atomic fluorescence spectrometry. Spectrochimica Acta Part B: Atomic Spectroscopy, 205 (2023), 106692, DOI: 10.1016/j.sab.2023.106692.

Appendix IV

B. ŠTÁDLEROVÁ, L. SAGAPOVA, S. MUSIL: Chemical vapour generation assisted by Cr^{3+}/KCN coupled to atomic fluorescence spectrometry for ultrasensitive determination of cadmium in water and rice samples. Journal of Analytical Atomic Spectrometry, 38 (2023), 1213–1223, DOI: 10.1039/d3ja00083d.